Timing of Lithospheric Extension in Northeastern China: Evidence from the Late Mesozoic Nianzishan A-Type Granitoid Complex

Jinhua Qin[1], **Cui Liu**[*,2], **Yuchuan Chen**[1], **Jinfu Deng**[2]

1. *MNR Key Laboratory of Metallogeny and Mineral Assessment, Institute of Mineral Resources, CAGS, Beijing* 100037, *China*
2. *School of Earth Sciences and Resources, China University of Geosciences, Beijing* 100083, *China*

Jinhua Qin: https://orcid.org/0000-0003-4646-2107

ABSTRACT: New zircon U-Pb dates obtained by laser ablation inductively coupled plasma mass spectrometry (LA-ICP-MS), whole-rock geochemical data and Sm-Nd and Rb-Sr isotopic data are presented for miarolitic alkaline granites, porphyritic syenite and rhyolites of the Nianzishan A-type granitoid complex (NAGC) in the Great Xing'an Range-Songliao Basin in Northeast (NE) China. New crystallization ages of 112.95±0.93 and 114.1±1.71 Ma for granite and 118.6±0.51 Ma for porphyritic syenite were determined by high-precision LA-ICP-MS. The $\varepsilon_{Nd}(t)$ of the rocks range from +1.85 to +2.06, with Nd model ages (T_{DM1}) from 671 to 821 Ma, indicating that the NAGC originated from juvenile source rocks and exhibits geochemical characteristics of A_1- and AA-type granite which formed in an extensional setting. We attribute the magmatism to regional extension and lithospheric thinning caused by the subduction of the western Pacific Plate about 120 to 100 Ma.
KEY WORDS: A-type granite, new zircon U-Pb zircon ages, NE China, lithospheric extension.

0 INTRODUCTION

The Nianzishan A-type granitoid complex (NAGC) is located in the Great Xing'an-Mongolian orogenic belt (XMOB) in NE China, at the eastern end of the Central Asian orogenic belt (CAOB) surrounded by the Siberian massif, Sino-Korean massif, and North China Craton (Ge et al., 1999; Şengör and Natal'in, 1996; Şengör et al., 1993). The complex evolution history and multiple collisions of micro-continental fragments since the Paleozoic make this an important site for studying the tectonic evolution of East Asia (Zhao et al., 2018; Xu et al., 2013; Wu et al., 2011; Zhang Y L et al., 2008).

Loiselle and Wones (1979) characterized A-type granites as anorogenic, mildly alkaline, with anhydrous affinities. Their occurrence has important tectonic implications, providing insights into post-collisional and intraplate extensional magmatic processes (Bornin, 2007; Frost et al., 2007; Liu et al., 2003; King et al., 1997; Eby, 1992, 1990; Creases et al., 1991; Whalen et al., 1987; Collins et al., 1982). Therefore, the Mesozoic A-type granites of NE China have received increasing attention and the NAGC should play a key role in understanding the history of regional extension in East Asia (Tian et al., 2014; Yang et al., 2006; Wu et al., 2002; Jahn et al., 2001).

A change in regional tectonics from compressional to extensional has occurred in NE China since Mesozoic times, but the timing of the transition is controversial. Previous studies suggested that the change had ceased by the Early Cretaceous and was followed by strong lithospheric thinning in the Late Cretaceous (130 to 120 Ma) (Wu et al., 2002; Jahn et al., 2001). The first age to be obtained from the NAGC was by a K-Ar method on biotite and K-feldspar and yielded Cretaceous ages of 123 Ma for miarolitic alkaline granite and 135 Ma for porphyritic syenite (Li and Yu, 1993), constraining the age of A-type granitic magmatism at around 130 Ma in an anorogenic extensional setting (Zhang, 2009; Wu et al., 2002; Jahn et al., 2001; Li and Yu, 1993). However, recent research has obtained younger ages of A-type granites than those reported previously, and the latest U-Pb zircon concordia ages of nearby A-type granites show a broad range from 100 to 120 Ma (Qiu et al., 2014; Qin et al., 2012; Wu et al., 2002). Better constrained dates should improve our understanding of tectonic setting.

We present new petrological, mineralogical, whole-rock geochemical data, Sr-Nd isotopes, and zircon U-Pb ages of the NAGC in this paper. Furthermore, in order to establish a tectonic framework for lithospheric extension and thinning in NE China since the Mesozoic, we have compiled ages of other Mesozoic igneous rocks from this region to construct a spatiotemporal pattern of tectonic evolution.

1 REGIONAL GEOLOGY

The Nianzishan A-type granitoid complex is located in the Great Xing'an Range, which is the eastern section of the CAOB. It is bounded by the Great Xing'an Range to the west and the Songliao Basin to the east (Fig. 1a). The regional tec-

tonics and magmatic activity are complex and mark the closure of sutures between several microcontinents (Zhao et al. 2017; Wu et al., 2011; Zhang et al., 2006). The study area is in the Huaan depression, the subzone between the Longjiang uplift and the Nenjiang depression, bounded by the Nenjiang-Balihan fault, the Great Xing'an fault, and the Xar Moron River fault. The Yalu River fault is closely spatially related to the NAGC and trends NW to NNW. Fault activity occurred during the Late Mesozoic to Cenozoic, and was significantly later than the formation age of the NAGC (Qian et al., 2018). Voluminous volcanic rocks occur in the area. The oldest volcanic stratigraphic units in the study area belong to the Laolongtou Group (T_{1l}) in the NW. Late Mesozoic volcanic units in the region comprise the Manitu Group (J_{3mn}), the Baiyingaolao Group (K_{1b}), and the Meiletu Group (K_{1m}). Sedimentary formations are the Dashizhai Group (P_{2d}), the Zhesi Group (P_{2z}), and Quaternary sediments. Intrusive magmatic rocks are common in the region and comprise Late Paleozoic and Early Mesozoic monzonitic granites related to the NE-SW closure and extension of the Paleo-Asian Ocean (Fig. 1b). Late Mesozoic A-type granite with typical miarolitic cavities is common in the region, and its genesis is attributed to subduction of the Pacific Plate. In addition, dyke swarms of granitic and dioritic porphyries are found within Late Mesozoic strata (K_{1b}).

2 PETROLOGY

The study area is near Qiqihaer City in Heilongjiang Province. The NAGC outcrops over an area of approximately

25 km^2, and is divided into a central and a marginal facies (Fig. 1b); the boundary between them is gradational. Fresh granite is pale-red and turns brown when weathered (Figs. 2a, 2c). The granite at the center of the complex is medium to coarse-grained with a roughly circular outcrop approximately 4 km in diameter. Miarolitic cavities with diameters from 0.5 to 2.0 cm are uniformly distributed within the coarse-grained granite and infilled with quartz and blue to black hornblende. The marginal facies is of porphyritic alkaline granite, located mainly to the north and southeast and in contact with Early Cretaceous rhyolite. We have not examined these contacts in this study. This fine-grained granite is often weathered from a light color to brown (Fig. 2d). The country rock rhyolite is glassy and contains quartz and plagioclase (15 vol.%).

Alkaline miarolitic granite: The alkaline miarolitic granite is porphyritic, consisting of alkali-feldspar with hypidiomorphic quartz, blue-green pleochroic arfvedsonite and aegirine. Apatite, zircon, and magnetite are accessory phases. Alkali-feldspar phenocrysts are hypidiomorphic to idiomorphic K-feldspar (~45 vol.%) and albite (~20 vol.%) crystals up to ~3 mm, suggesting early crystallization. Feldspar grains have undergone sericitization and kaolinization. Interstitial, subhedral to anhedral quartz grains ranging from 1 to 2 mm in size constitute ~30 vol.% of the granite. Amphibole crystals range from 0.5 to 0.8 mm in size and constitute 5 vol.% to 10 vol.% of the granite. Pyroxene rims are observed around the amphibole grains. The acicular to fibrous amphibole is pleochroic from light brown to dark green. It contains 47.84 wt.% to 51.69 wt.%

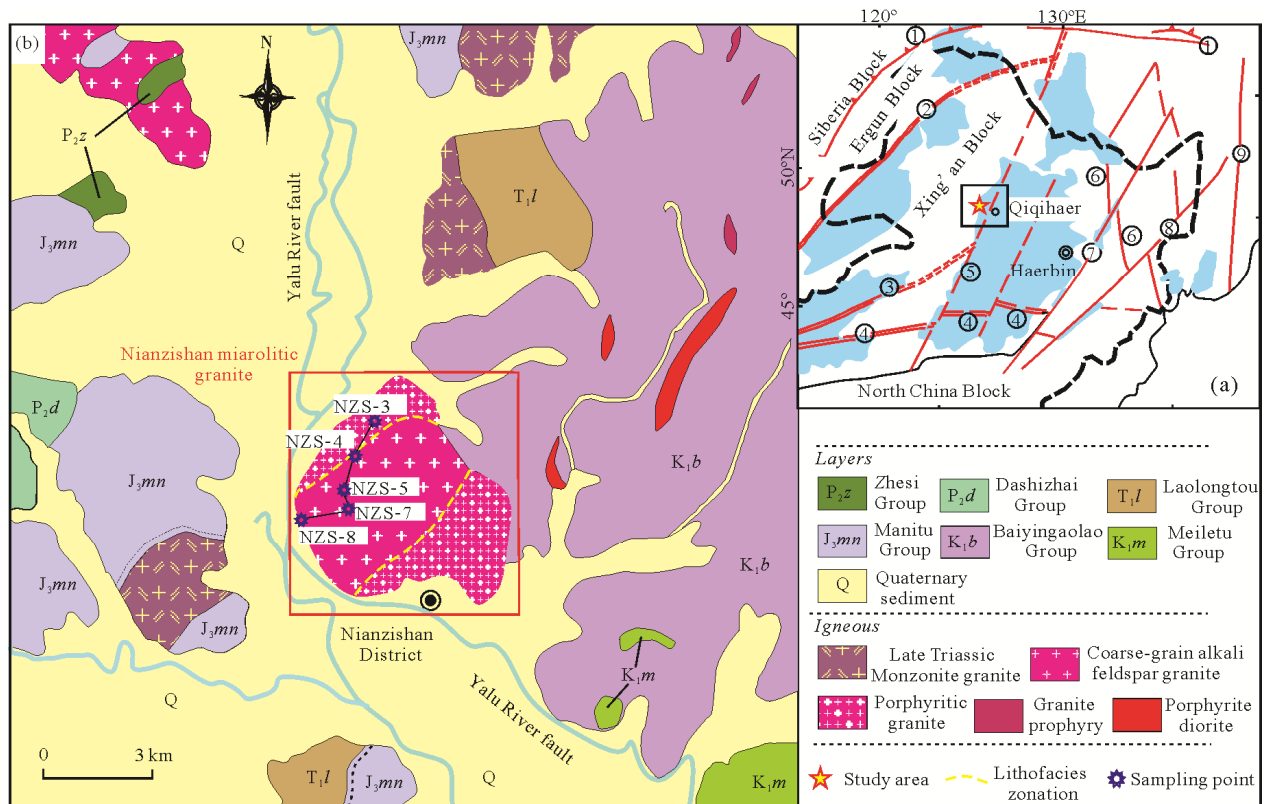**Figure 1.** (a) Regional tectonic map of NE China (after Zhang et al., 2006). ① Mongolia-Okhotsk suture zone; ② Deerbugan fault; ③ Hegenshan fault; ④ Xilamulun fault; ⑤ Nenjiang-Balihan fault; ⑥ Mudanjiang fault; ⑦ Jiamusi-Yitong fault; ⑧ Dunhua-Mishan fault; ⑨ Xilinhot-Alin central belt; (b) schematic geological map of the NAGC and surrounding area (Regional Geological Survey of Heilongjiang Province, China, unpublished).

SiO_2, 33.74 wt.% to 35.71 wt.% FeO, and 7.20 wt.% to 7.87 wt.% Na_2O. On the basis of 23 oxygen atoms, Si is 7.856 to 8.270, A/(Na+K) is 0.796 to 1.187, and Ca_B is 0.043 to 0.235, indicating that the amphibole is typical arfvedsonite (Leake et al., 1997). Pyroxene contains 52.82 wt.% to 52.93 wt.% SiO_2, 31.3 wt.% to 37.81 wt.% FeO, and 12.51 wt.% to 12.87 wt.% Na_2O. Its orthoferrosilite (Fs) content is 49.4 wt.% to 50.0 wt.%, acmite (Ac) is 49.2 wt.% to 49.7 wt.%, and the rest is wollastonite (Wo) and enstatite (En). It is classified as acmite (Morimoto, 1988) (Figs. 2b, 2d).

Porphyritic syenite enclosures (sample NZS-7): Syenite enclosures 2 to 50 mm in size are common in the granite. They consist of fine-grained porphyritic syenite containing ca. 7-mm phenocrysts of K-feldspar (40 vol.%), plagioclase (5 vol.% to 10 vol.%), quartz (<5 vol.%), and fine-grained groundmass (50 vol.%) (Fig. 2e).

Rhyolite (sample NZS-8): The rhyolite is porphyritic with dark gray phenocrysts, consisting of quartz (10 vol.% to 15 vol.%), and feldspar (5 vol.%) with grain sizes from 0.5 to 1 mm. Most quartz grains are angular and rounded at the margins. The groundmass (70 vol.% to 80 vol.%) is microcrystalline to cryptocrystalline or glassy (Fig. 2f).

3 SAMPLING AND ANALYTICAL METHODS

Five samples were collected from the NAGC for analysis: three samples of miarolitic granite (NZS-3, NZS-4, and NZS-5); one porphyritic syenite (NZS-7); and one rhyolite (NZS-8). All samples were little weathered and appropriate for whole-rock geochemistry and Sr-Nd isotope analyses. Samples NZS-3, NZS-4 and NZS-7 were selected for geochronological dating.

3.1 LA-ICP-MS U-Pb Dating

Zircon grains were separated from samples NZS-3, NZS-4 and NZS-7 for U-Pb age dating. The bulk samples were crushed to 60 to 80 meshes size, and zircons were separated using gravity and electromagnetic techniques and finally hand-picked under a binocular microscope. The zircon crystals were then mounted on epoxy resin, smoothed and polished, and finally gold coated. They were examined using transmitted and reflected light and cathodoluminescence (CL) microscopy.

Zircon U-Pb ages were determined at the Institute of Mineral Resources, CAGS, Beijing, using a Finnigan, Neptune ICP-MS with a New Wave UP213 laser-ablation system. Helium was used as the carrier gas, and the beam diameter was 30 μm with a 10-Hz repetition rate and a laser power of 2.5 J/cm^2. Eight ion counters were used to receive ^{238}U, ^{235}U, ^{232}Th, ^{208}Pb, ^{207}Pb, ^{206}Pb, ^{204}Pb, and ^{202}Hg signals simultaneously, while data for ^{208}Pb, ^{232}Th, ^{235}U, and ^{238}U were collected in a Faraday cage. Zircon GJ-1 was used as standard, and Plešovice zircon was used to calibrate the mass spectrometer. U, Th, and Pb concentrations were calibrated using ^{29}Si as internal standard and zircon M127 (U: 923 ppm; Th: 439 ppm; Th/U: 0.475, Nasdala et al., 2008) as external standard. $^{207}Pb/^{206}Pb$ and $^{206}Pb/^{238}U$ were calculated using the ICP-MS DataCal 4.3 program. No correction was made for common Pb because of a high $^{206}Pb/^{204}Pb$ ratio. Abnormally high ^{204}Pb data were deleted. The Plešovice zircon was dated as unknown and yielded a weighted mean $^{206}Pb/^{238}U$ age of 337±2 Ma (2SD, n=12), which is in good agreement with the recommended $^{206}Pb/^{238}U$ age of 337.13± 0.37 Ma (2SD) (Sláma et al. 2008). Age calculations were performed, and concordia diagrams generated using the Isoplot/Ex 3.0 software (Ludwig, 2003).

3.2 Major and Trace Elements

Major and trace elements were analyzed at the Hubei Testing Center, Wuhan. Relatively fresh samples were selected after examination in thin section under the microscope, sawn into slabs, and the central parts were used in whole-rock analysis. Specimens were crushed in a steel mortar and ground in a steel mill to powders of ~200 meshes. Major elements were
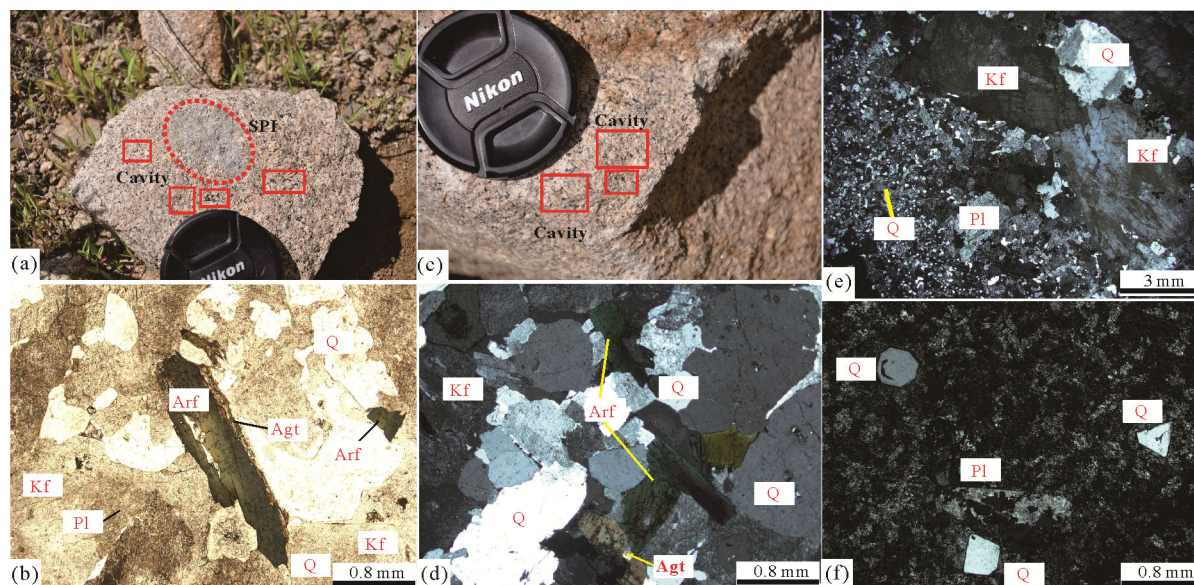

Figure 2. (a) and (c) field photographs, camera lens cap 67 mm diameter. (a)–(d) Miarolitic alkaline granite; (e) porphyritic syenite enclosure; (f) rhyolite. Q. Quarz; Kf. orthoclase; Pl. plagioclase; Arf. arfvedsonite; Agt. aegirine-augite. Dashed red line in (a) surrounds a microporphyritic syenite enclosure; (b) in plane-polarized light; (d), (e), (f) between crossed polars.

analyzed by X-ray fluorescence spectroscopy using the methods of Norrish and Chappell (1977), and ferric and ferrous iron were determined using wet chemical methods.

Trace elements were determined in solution by ICP-MS at the National Research Center for Geoanalysis, Beijing. Approximately 40 mg of sample was dissolved in distilled $HF+HClO_4$ in 15 mL Savillex Teflon screw-cap beakers. Analytical precision for most elements was typically better than 5% relative standard deviation (RSD), and the measured values for Zr, Hf, Nb, and Ta were within 10% of the certified values. The sample preparation and instrument operation and calibration were described by Qi et al. (2000).

3.3   Sr-Nd Isotope Analysis

Sr-Nd isotope analyses were performed using a Finnigan MAT262 mass spectrometer at China University of Geosciences, Beijing. Approximately 50 mg of whole-rock powdered sample were dissolved in a Teflon bomb using a mixture of HF and HNO_3. Sr and rare earth elements (REE) were isolated using a 0.2 mL column filled with Sr and REE-Spec resins (manufactured by Eichrom Industries, Inc.) for selective extraction of Sr and REE, respectively. Nd fractions were further separated and purified using LN resin with HCl as eluent. Procedures for performing mass analyses followed those described by Qiao (1988). Rb and Sr mass fractionations were calibrated using $^{86}Sr/^{88}Sr=0.119\ 4$, and Sr blank was <100 pg during the entire process. The $^{87}Sr/^{86}Sr$ of the standard is 0.710 248±0.000 011. Nd blank was <500 pg, and the $^{143}Nd/^{144}Nd$ of the standard was 0.512 111±0.000 011 (2σ, n=10); a $^{146}Nd/^{144}Nd=0.721\ 9$ correction was applied to $^{143}Nd/^{144}Nd$.

4   RESULTS
4.1   Zircon U-Pb Chronology

The zircon grains of samples NZS-3 and NZS-4 exhibit length-to-width ratios between 1 : 1 and 2 : 1 and are 100 to 300 μm in size. Most zircon grains have oscillatory zoning (Fig. 3), suggesting an igneous origin. U content is from 48 ppm to 523 ppm, Th content is from 38 ppm to 543 ppm, and Th/U ratio is >0.4; all these values are characteristic of typical magmatic zircons (Schulz et al., 2006; Wu and Zhen, 2004; Rubatto, 2002).

The length-to-width ratios of zircon grains in sample NZS-7 and their internal structures are similar to those of the alkaline granite (2 : 1) and are overall >100 μm (Fig. 3). U contents vary between 34 ppm and 3 525 ppm and Th between 48 ppm and 1 689 ppm; zircon Th/U averaged approximately 0.86. The zircons are grouped into (1) light-colored with U of 71.3 ppm to 357.11 ppm and Th of 75.2 ppm to 358.09 ppm

and (2) dark with metamictization and U of 1 365.1 ppm to 1 697.3 ppm and Th of 423.69 ppm to 2 500.3 ppm.

4.1.1   Miarolitic alkaline granite (NZS-3 and NZS-4)

Nineteen out of thirty spot analyses of the miarolitic granite sample NZS-3 yielded $^{206}Pb/^{238}U$ ages of 107 to 133 Ma, with a concordia U-Pb age of 112.95±0.93 Ma (MSWD=1.14). This age provides the best estimate for the crystallization age of the NAGC (Fig. 4a). Thirteen spot analyses of the miarolitic granite sample NZS-4 yielded $^{206}Pb/^{238}U$ ages of 96 to 135 Ma and a concordia U-Pb age of 114.1±1.7 Ma (MSWD=0.72) (Fig. 4b). Two samples collected from different parts of the rock exhibited almost identical ages within analytical errors. Thus, the Nianzhishan A-type granitic magmatism is Late Cretaceous in age.

4.1.2   Porphyritic syenite inclusion (NZS-7)

Twenty-nine spot analyses yielded $^{206}Pb/^{238}U$ ages ranging from 102 to 131 Ma. The ages for the two zircon groups overlap each other. The age of the light-colored group ranges from 102 to 131 Ma, whereas that of the dark group ranges from 118±1 to 119±1 Ma. Seven of analyses are concordant or nearly concordant and cluster as a single population with weighted mean $^{206}Pb/^{238}U$ age of 118.6±0.51 Ma (MSWD=8.6) (Fig. 4c). Since the porphyritic syenite occurs as an inclusion within the granite, this age suggests that it crystallized somewhat earlier than the granite.

4.2   Geochemistry
4.2.1   Major elements

Table 1 lists major and trace element analyses. Miarolitic alkaline granite (samples NZS-3–5) has high SiO_2 (71.98 wt.% to 72.90 wt.%), FeO^T (2.96 wt.% to 3.39 wt.%), and K/Na >1; its alkali content is 8 wt.% to 10 wt.%, FeO^T/MgO ratios range 23 to 34, Al_2O_3 is less than 13 wt.%, A/CNK is from 0.95 to 1.01, and A/NK ratio is from 1.0 to 1.04. CIPW normative minerals yield a quartz content of 23.60 wt.% to 27.25 wt.%, plagioclase of 0.5 wt.% to 4 wt.%, alkali-feldspar of 63.2 wt.% to 70.6 wt.%, corundum <1 wt.%, and pyroxene >2 wt.%. The porphyritic syenite inclusion (sample NZS-7) has concentrations of 67.47 wt.% SiO_2, 17 wt.% Al_2O_3, 0.24 wt.% MgO, 0.41 wt.% CaO, 5.50 wt.% Na_2O, and 6.22 wt.% K_2O and is characterized by high ALK (Na_2O+K_2O) (11 wt.%), and high K/Na ratio (1.13), A/CNK ratio of 1.01 and A/NK ratio of 1.05 point to a weakly peraluminous rock. CIPW normative minerals yielded 10.55 wt.% of quartz, 81.96 wt.% of alkali-feldspar, and 3.99 wt.% of plagioclase. Rhyolite (sample NZS-8) is similar to granite in composition, with high SiO_2 and ALK and low

115±3 Ma   116±2 Ma   111±1 Ma   109±3 Ma   110±4 Ma   112±2 Ma   118±4 Ma   131±5 Ma   103±5 Ma

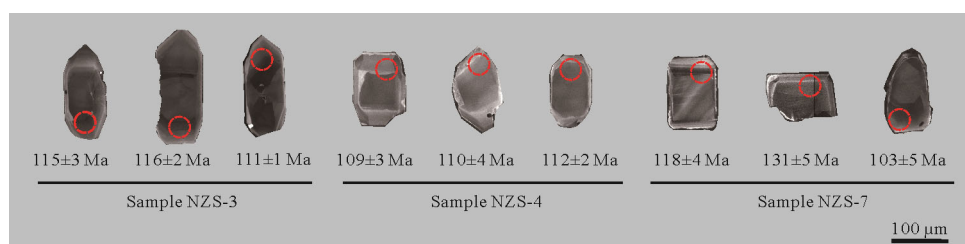Sample NZS-3   Sample NZS-4   Sample NZS-7

100 μm

Figure 3. Cathodoluminescence images of selected typical zircon grains.

Table 1 LA-ICP-MS zircon U-Pb results of the Nianzishan A-type granitic composite (n.d.: not detected)

Spot	$W_B/10^{-6}$			Th/U	Isotope ratio ($\pm 1\sigma$)						Isotope age (Ma) ($\pm 1\sigma$)					
	Pb	Th	U		$^{207}Pb/^{206}Pb$		$^{207}Pb/^{235}U$		$^{206}Pb/^{238}U$		$^{207}Pb/^{206}Pb$		$^{207}Pb/^{235}U$		$^{206}Pb/^{238}U$	
					Ratio	Erro	Ratio	Erro	Ratio	Erro	Age	Erro	Age	Erro	Age	Erro
NZS-3																
NZS-3-1	11.66	543.1	486.84	1.12	0.050 284	0.001 8	0.119 2	0.004 0	0.017 4	0.000 2	209.33	81.47	114.30	3.64	111.23	0.99
NZS-3-2	3.05	82.58	137.41	0.60	0.051 477	0.006 2	0.125 2	0.013 2	0.018 0	0.000 5	261.18	255.5	119.74	11.93	114.76	3.19
NZS-3-3	3.82	122.75	185.25	0.66	0.050 520	0.007 1	0.118 0	0.0177	0.016 8	0.000 9	220.44	296.3	113.29	16.07	107.19	5.97
NZS-3-4	5.19	167.41	231.46	0.72	0.051 547	0.003 0	0.123 9	0.007 5	0.017 6	0.000 3	264.88	131.5	118.59	6.81	112.36	1.99
NZS-3-5	6.19	222.51	275.53	0.81	0.049 789	0.003 0	0.118 6	0.007 0	0.017 5	0.000 3	183.42	142.6	113.83	6.38	112.01	1.59
NZS-3-6	3.8	113.8	176.99	0.64	0.053 657	0.007 2	0.119 3	0.015 3	0.017 1	0.001 0	366.72	300.9	114.41	13.91	109.01	6.09
NZS-3-7	3.67	103.87	168.18	0.62	0.051 602	0.007 6	0.123 4	0.014 3	0.017 7	0.000 6	333.39	238.9	118.19	12.97	113.41	3.69
NZS-3-8	9.69	396.51	410.48	0.97	0.051 781	0.002 3	0.123 8	0.005 1	0.017 7	0.000 2	275.99	99.99	118.52	4.61	113.02	1.17
NZS-3-9	4.03	118.77	181.47	0.65	0.064 658	0.003 1	0.158 1	0.007 3	0.018 1	0.000 3	764.82	101.8	149.02	6.39	115.6	1.85
NZS-3-10	7.35	259.14	312.38	0.83	0.051 956	0.003 8	0.128 6	0.008 9	0.018 1	0.000 4	283.4	168.5	122.81	8.00	115.87	2.30
NZS-3-11	6.53	206.42	273.93	0.75	0.051 821	0.006 9	0.130 6	0.015 2	0.019 1	0.001 0	275.99	290.7	124.68	13.65	121.78	6.38
NZS-3-12	2.17	38.92	81.41	0.48	0.159 947	0.041 9	0.470 9	0.039 6	0.020 2	0.000 8	2 455.2	457.4	391.8	27.38	128.85	4.98
NZS-3-13	12.16	513.43	514.22	1.00	0.050 362	0.002 0	0.119 3	0.004 3	0.017 7	0.000 2	213.04	92.58	114.46	3.88	113.15	1.33
NZS-3-14	6.21	180.54	281.35	0.64	0.053 490	0.005 9	0.128 6	0.012 1	0.018 0	0.000 4	350.06	254.6	122.86	10.89	115.05	2.82
NZS-3-15	5.65	135.86	234.84	0.58	0.050 165	0.003 9	0.144 1	0.012 0	0.020 9	0.000 5	211.19	179.6	136.72	10.64	133.13	3.47
NZS-3-16	1.88	36.98	85.03	0.43	0.130 192	0.012 5	0.310 2	0.019 8	0.020 1	0.000 5	2 101.9	169.9	274.36	15.36	128.47	3.15
NZS-3-17	4.41	139.42	211.69	0.66	0.051 483	0.006 2	0.125 2	0.014 8	0.018 1	0.000 5	261.18	255.5	119.76	13.38	115.42	2.89
NZS-3-18	2.91	79.33	139.38	0.57	0.071 720	0.005 9	0.173 3	0.013 4	0.018 1	0.000 5	988.89	169.6	162.27	11.64	115.64	3.12
NZS-3-19	3.05	87.41	126.19	0.69	0.118 900	0.009 8	0.285 2	0.017 2	0.018 8	0.000 4	1 939.8	148.1	254.79	13.63	120.29	2.63
NZS-3-20	2.01	52.59	92.8	0.57	0.115 549	0.015 4	0.261 9	0.023 2	0.019 0	0.000 7	1 888.6	247.2	236.22	18.71	121.42	4.71
NZS-3-21	5.99	229.23	289.33	0.79	0.050 770	0.005 0	0.117 0	0.010 8	0.017 3	0.000 4	231.55	211.1	112.39	9.79	110.88	2.36
NZS-3-22	2.9	77.11	133.45	0.58	0.086 612	0.007 2	0.210 2	0.015 4	0.019 0	0.000 6	1 353.7	160	193.72	12.93	121.31	3.66
NZS-3-23	8.19	335.85	365.9	0.92	0.050 067	0.002 9	0.124 2	0.007 3	0.018 2	0.000 3	198.23	137	118.85	6.62	116.33	1.60
NZS-3-24	n.d.	n.d.	n.d.	n.d.	1.101 484	n.d.	n.d.	n.d.	n.d.	n.d.	n.d.	n.d.	n.d.	n.d.	n.d.	n.d.
NZS-3-25	11.59	600.12	523.98	1.15	0.052 950	0.004 4	0.120 3	0.009 8	0.016 9	0.000 4	327.84	188.9	115.39	8.84	108.18	2.81
NZS-3-26	2.5	56.12	116.76	0.48	0.071 621	0.006 1	0.172 1	0.012 3	0.018 3	0.000 8	975.93	174.5	161.2	10.70	116.67	4.94
NZS-3-27	2.28	63.85	113.37	0.56	0.049 452	0.003 7	0.118 6	0.004 2	0.017 6	0.001 3	168.6	175.9	113.84	3.84	112.22	8.16
NZS-3-28	5.6	199.61	218.4	0.91	0.067 928	0.003 6	0.184 7	0.009 3	0.020 0	0.000 3	866.35	110.3	172.08	7.98	127.82	1.65
NZS-3-29	7.35	294.46	331.42	0.89	0.052 017	0.007 0	0.127 1	0.015 5	0.018 2	0.000 6	287.1	281.5	121.49	13.96	116.22	4.01
NZS-3-30	2.93	81.08	125.98	0.64	0.047 648	0.005 0	0.125 7	0.015 4	0.018 7	0.000 8	83.425	238.9	120.24	13.85	119.55	5.01

Jinhua Qin, Cui Liu, Yuchuan Chen and Jinfu Deng

Table 1 Continued

Spot	W_B/10^-6			Th/U	Isotope ratio (±1σ)						Isotope age (Ma) (±1σ)					
	Pb	Th	U		$^{207}Pb/^{206}Pb$ Ratio	Erro	$^{207}Pb/^{235}U$ Ratio	Erro	$^{206}Pb/^{238}U$ Ratio	Erro	$^{207}Pb/^{206}Pb$ Age	Erro	$^{207}Pb/^{235}U$ Age	Erro	$^{206}Pb/^{238}U$ Age	Erro
NZS-4																
NZS-4-1	2.35	55	78.23	0.70	0.149 735	0.015 8	0.385 7	0.038 7	0.021 1	0.001 1	2 342.9	181.2	331.22	28.34	134.55	6.71
NZS-4-2	2.10	54.49	102.35	0.53	0.090 327	0.009 2	0.199 8	0.020 6	0.016 7	0.000 6	1 432.4	195.8	184.96	17.44	106.86	3.81
NZS-4-3	4.52	142.1	212.26	0.67	0.055 061	0.008 5	0.124 3	0.015 5	0.017 6	0.000 8	413.01	348.1	118.97	13.96	112.23	5.06
NZS-4-4	4.64	143.11	215.08	0.67	0.054 157	0.008 7	0.130 3	0.017 4	0.018 1	0.000 7	375.98	325.9	124.33	15.61	115.69	4.52
NZS-4-5	1.64	68.48	74.79	0.92	0.156 703	0.013 9	0.363 3	0.031 2	0.018 0	0.000 6	2 420.7	151.7	314.7	23.28	115.26	3.76
NZS-4-6	4.29	139.58	213.51	0.65	0.051 843	0.007 5	0.118 2	0.016 7	0.016 9	0.001 1	279.69	309.2	113.46	15.14	107.89	6.66
NZS-4-7	2.21	54.93	122.66	0.45	0.113 212	0.014 0	0.207 4	0.018 9	0.015 1	0.000 6	1 851.6	225.8	191.4	15.89	96.492	3.90
NZS-4-8	1.36	41.42	63.97	0.65	0.121 298	0.013 7	0.306 7	0.028 0	0.018 2	0.000 9	1 975.9	202.9	271.63	21.80	116.04	5.98
NZS-4-9	4.98	180.37	213.5	0.84	0.055 941	0.007 3	0.131 6	0.015 2	0.018 5	0.000 7	450.05	292.6	125.58	13.65	118.06	4.59
NZS-4-10	1.53	32.60	72.70	0.45	0.137 111	0.009 5	0.308 1	0.017 6	0.018 2	0.000 5	2 191.1	121.3	272.67	13.64	116.48	3.37
NZS-4-11	5.21	181.01	245.44	0.74	0.053 941	0.006 2	0.125 9	0.012 7	0.017 7	0.000 6	368.57	262.9	120.4	11.45	113.32	3.89
NZS-4-12	2.30	58.80	104.18	0.56	0.090 867	0.011 6	0.234 5	0.024 4	0.018 9	0.000 8	1 443.5	240	213.91	20.04	120.52	4.99
NZS-4-13	2.71	76.38	124.48	0.61	0.088 946	0.007 8	0.213 4	0.016 7	0.018 7	0.000 4	1 402.8	169.1	196.39	13.95	119.32	2.79
NZS-4-14	1.73	42.32	81.38	0.52	0.128 987	0.012 8	0.289 6	0.021 7	0.018 5	0.000 5	2 084.3	175.8	258.23	17.11	118.36	3.17
NZS-4-15	1.15	24.28	56.18	0.43	0.130 706	0.008 6	0.307 8	0.020 1	0.018 3	0.000 6	2 109.3	116.8	272.45	15.63	117.04	3.69
NZS-4-16	2.89	89.47	143.17	0.62	0.073 662	0.004 2	0.177 6	0.009 5	0.017 6	0.000 4	1 031.5	111	165.95	8.18	112.41	2.36
NZS-4-17	6.3	216.21	261.94	0.83	0.059 750	0.005 9	0.155 8	0.014 5	0.019 6	0.000 5	594.47	214.8	147.05	12.72	124.97	3.12
NZS-4-18	1.79	47.26	88.03	0.54	0.107 539	0.008 9	0.242 7	0.016 0	0.017 7	0.000 4	1 758.3	152.3	220.62	13.08	112.88	2.62
NZS-4-19	4.52	160.55	223.84	0.72	0.053 151	0.004 7	0.119 0	0.009 1	0.016 9	0.000 4	344.5	201.8	114.2	8.29	108.03	2.71
NZS-4-20	1.38	29.32	67.14	0.44	0.132 534	0.016 2	0.310 9	0.029 6	0.017 6	0.001 1	2 131.8	214.7	274.86	22.93	112.23	7.18
NZS-4-21	0.88	20.61	48.13	0.43	0.395 919	0.099 8	0.363 2	0.026 4	0.016 1	0.000 9	3 893.7	389.2	314.57	19.70	103.18	5.54
NZS-4-22	3.50	110.66	168.39	0.66	0.051 617	0.005 7	0.123 4	0.012 2	0.017 7	0.000 6	333.39	168.5	118.12	11.06	113.33	3.50
NZS-4-23	6.95	274.72	304.81	0.90	0.051 584	0.002 0	0.125 9	0.004 7	0.018 1	0.000 2	333.39	88.88	120.38	4.28	115.32	1.25
NZS-4-24	2.94	80.93	138.46	0.58	0.056 395	0.008 7	0.128 3	0.021 7	0.018 4	0.001 2	477.82	346.3	122.54	19.49	117.74	7.34
NZS-4-25	2.14	54.32	107.36	0.51	0.055 781	0.006 3	0.132 4	0.001 6	0.018 0	0.001 3	442.64	251.8	126.26	1.44	115.08	8.04
NZS-4-26	1.48	30.76	75.57	0.41	0.107 758	0.013 4	0.235 7	0.024 1	0.017 2	0.000 6	1 762	228.2	214.89	19.81	110.16	3.65
NZS-4-27	1.59	39.38	79.49	0.5	0.106 428	0.010 4	0.233 7	0.023 2	0.017 2	0.000 5	1 739.2	179.6	213.21	19.10	109.87	3.47
NZS-4-28	3.17	97.46	156.59	0.62	0.054 554	0.012 0	0.116 3	0.016 4	0.017 4	0.000 9	394.5	438.8	111.71	14.90	111.24	5.67
NZS-4-29	2.45	68.96	117.96	0.58	0.047 847	0.007 6	0.129 4	0.025 4	0.018 3	0.001 1	100.09	331.4	123.6	22.83	117.2	6.93
NZS-4-30	4.51	138.63	205.50	0.67	0.053 713	0.004 3	0.131 8	0.009 9	0.017 9	0.000 4	366.72	179.6	125.75	8.85	114.56	2.34

Table 1 Continued

Spot	$W_B/10^{-6}$			Th/U	Isotope ratio (±1σ)						Isotope age (Ma) (±1σ)					
	Pb	Th	U		$^{207}Pb/^{206}Pb$		$^{207}Pb/^{235}U$		$^{206}Pb/^{238}U$		$^{207}Pb/^{206}Pb$		$^{207}Pb/^{235}U$		$^{206}Pb/^{238}U$	
					Ratio	Erro	Ratio	Erro	Ratio	Erro	Age	Erro	Age	Erro	Age	Erro
NZS-7																
NZS-7-1	4.69	181.62	242.95	0.75	0.054 958	0.006 5	0.114 1	0.012 9	0.016 1	0.000 7	409.31	264.8	109.74	11.79	102.89	4.54
NZS-7-2	3.77	141.13	163.98	0.86	0.072 668	0.004 8	0.183 6	0.011 5	0.018 9	0.000 4	1 005.6	134.1	171.12	9.89	120.86	2.37
NZS-7-3	8.67	416.41	357.11	1.17	0.051 177	0.007 6	0.126 4	0.015 9	0.018 6	0.000 6	255.62	311.1	120.84	14.30	118.89	3.85
NZS-7-4	5.18	159.85	238.15	0.67	0.048 726	0.007 2	0.130 4	0.020 9	0.018 2	0.000 7	200.08	250	124.46	18.75	116.28	4.20
NZS-7-5	8.47	358.09	371.29	0.96	0.051 817	0.002 4	0.130 1	0.005 6	0.018 5	0.000 2	275.99	110.2	124.21	5.03	118.12	1.55
NZS-7-6	5.93	192.34	243.11	0.79	0.065 827	0.003 2	0.181 2	0.008 4	0.020 4	0.000 3	1 200	100	169.07	7.18	130.11	1.85
NZS-7-7	61.61	112.06	83.42	1.34	0.758 708	0.012 4	21.20	0.524 7	0.203 7	0.004 5	error	error	3147.8	24.00	1195.4	23.95
NZS-7-8	3.99	183.5	175.62	1.04	0.048 601	0.011 5	0.132 5	0.039 7	0.018 2	0.001 1	127.87	477.7	126.33	35.60	116.45	6.93
NZS-7-9	3.39	108.22	158.77	0.68	0.052 122	0.005 4	0.128 2	0.013 0	0.019 0	0.000 8	300.06	237	122.45	11.66	121.44	4.84
NZS-7-10	2.64	75.72	124.44	0.61	0.096 303	0.009 7	0.221 9	0.012 2	0.018 7	0.000 4	1 553.7	190.7	203.48	10.12	119.59	2.49
NZS-7-11	4.65	171.79	210.76	0.82	0.052 547	0.005 4	0.132 0	0.012 5	0.018 6	0.000 5	309.32	235.2	125.86	11.21	118.51	3.14
NZS-7-12	1.12	34.44	48.93	0.7	0.199 430	0.022 2	0.395 5	0.037 9	0.019 7	0.000 7	2 821.3	182.7	338.35	27.61	125.52	4.70
NZS-7-13	3.94	142.68	175.15	0.81	0.059 753	0.014 6	0.132 5	0.022 6	0.018 7	0.001 4	594.47	457.1	126.3	20.31	119.45	9.06
NZS-7-14	4.77	158.48	221.57	0.72	0.048 844	0.004 7	0.125 9	0.013 6	0.018 5	0.000 6	138.98	211.1	120.38	12.24	118.22	3.72
NZS-7-15	1.62	40.52	83.51	0.49	0.125 225	0.020 3	0.277 1	0.038 2	0.016 5	0.000 7	2 031.8	286	248.38	30.39	105.24	4.53
NZS-7-16	4.37	151.21	212.36	0.71	0.050 804	0.005 8	0.121 7	0.013 5	0.017 8	0.000 7	231.55	244.4	116.64	12.22	113.73	4.55
NZS-7-17	5.01	188	221.85	0.85	0.052 715	0.003 2	0.131 9	0.007 7	0.018 6	0.000 3	316.73	141.6	125.8	6.89	118.86	2.05
NZS-7-18	8.43	432.69	336.1	1.29	0.051 954	0.002 1	0.131 9	0.005 1	0.018 6	0.000 2	283.4	92.58	125.84	4.55	119.08	1.33
NZS-7-19	1.58	36.46	74.54	0.49	0.107 599	0.006 4	0.275 9	0.013 8	0.019 0	0.000 4	1 759	109.1	247.41	10.96	121.62	2.42
NZS-7-20	1.70	39.54	83.92	0.47	0.143 160	0.014 1	0.302 6	0.022 2	0.017 7	0.000 5	2 265.7	171.5	268.4	17.28	113.02	3.23
NZS-7-21	4.82	160.5	221.11	0.73	0.055 985	0.008 6	0.132 2	0.014 9	0.018 6	0.000 5	450.05	340.5	126.1	13.35	119.1	3.25
NZS-7-22	2.28	62.28	95.84	0.65	0.104 939	0.008 3	0.259 0	0.016 5	0.020 0	0.000 6	1 713.3	146.3	233.88	13.32	127.35	3.59
NZS-7-23	2.25	58.7	96.31	0.61	0.085 187	0.008 7	0.229 5	0.024 1	0.020 5	0.000 9	1 320.4	198.3	209.78	19.90	131.05	5.59
NZS-7-24	3.18	113.34	147.42	0.77	0.061 516	0.016 8	0.128 2	0.024 6	0.017 7	0.001 1	657.42	509.3	122.51	22.11	113.07	6.99
NZS-7-25	1.52	33.27	71.33	0.47	0.110 579	0.009 8	0.269 3	0.017 2	0.019 2	0.000 6	1 809.3	161.6	242.12	13.77	122.58	3.52
NZS-7-26	41.25	2 500.3	1568.6	1.59	0.050 225	0.001 0	0.130 0	0.002 7	0.018 7	0.000 1	205.63	41.66	124.12	2.45	119.41	0.75
NZS-7-27	48.29	3 525	1697.3	2.08	0.050 452	0.001 8	0.129 5	0.004 3	0.018 7	0.000 2	216.74	81.47	123.65	3.91	119.34	1.07
NZS-7-28	4.87	155.82	226.35	0.69	0.054 680	0.004 3	0.133 0	0.009 2	0.018 4	0.000 3	398.2	175.9	126.76	8.24	117.36	1.95
NZS-7-29	33.53	1826.9	1365.1	1.34	0.051 048	0.001 8	0.129 1	0.004 3	0.018 4	0.000 2	242.66	78.69	123.26	3.89	117.64	1.11
NZS-7-30	4.37	139.35	201.25	0.69	0.053 515	0.008 8	0.133 3	0.019 5	0.018 9	0.000 6	350.06	333.3	127.07	17.44	120.45	3.85
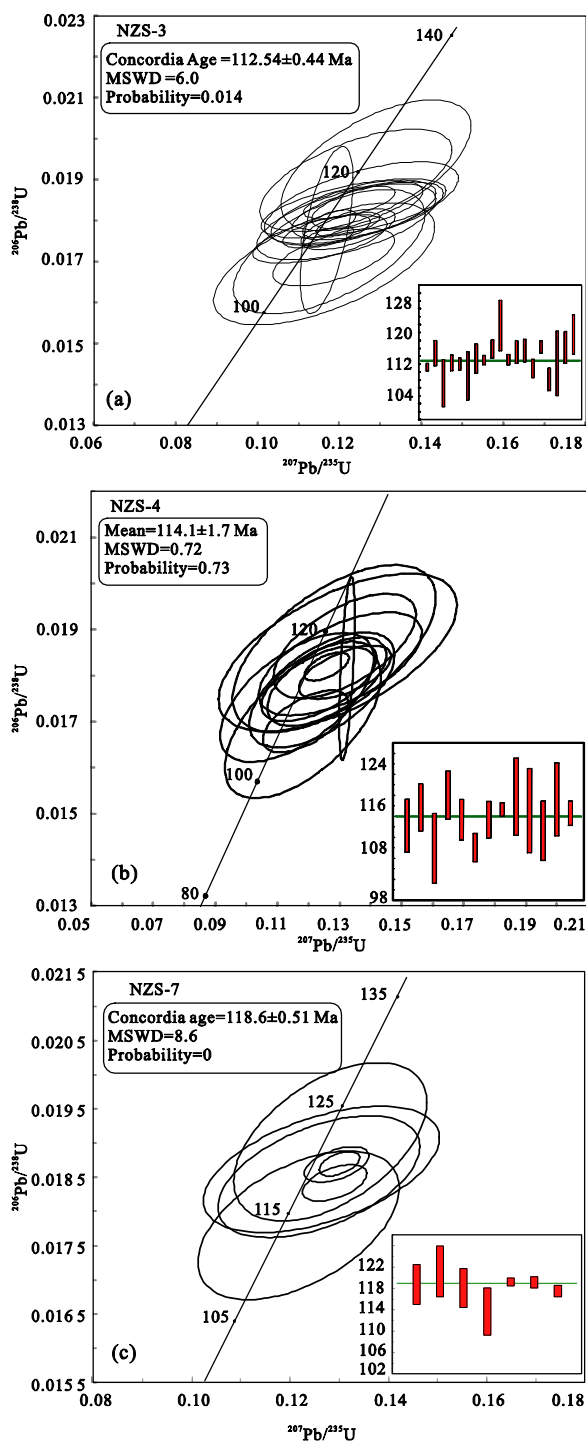
Figure 4. Zircon U-Pb concordia diagrams of the NAGC obtained by LA-ICP-MS; NZS-3, NZS-4. miarolitc alkaline granite; NZS-7. porphyrite syenite.

Al$_2$O$_3$, MgO, CaO, Mn, Ti, and P contents. Total FeO and FeO^T/ MgO are lower than those in the granite. A/CNK and A/NK ratio are 1.19 and 1.24, respectively. The CIPW normative minerals are quartz (39.7 wt.%); alkali-feldspar (54.54 wt.%); plagioclase feldspar (2.1 wt.%), and with corundum >1 wt.%.

Granite and syenite affinities are displayed in Fig. 5 and calc-alkaline and alkaline (AC) affinities in Fig. 6. Samples of the NAGC have similar geochemical properties to other granitoids in the Great Xing'an-Songliao Basin in Northeast China
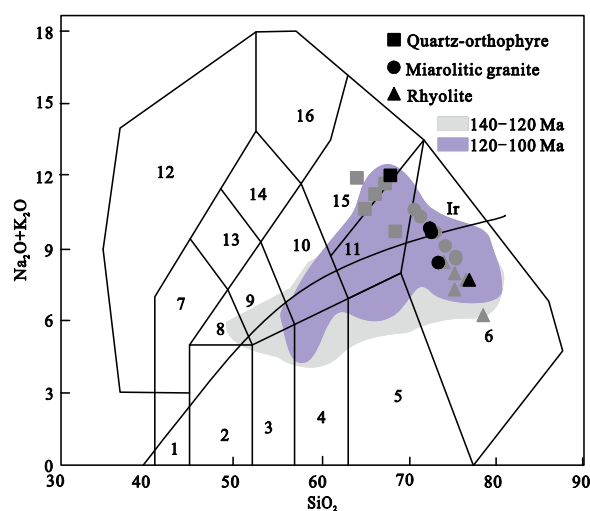
Figure 5. Total alkali-silica (TAS) classification diagram (Middlemost, 1994) of the NAGC major element analyses (Table 2). 1. olivine gabbro; 2. gabbro; 3. gabbroic diorite; 4. diorite; 5. granodiorite; 6. granite; 7. foidmonzo-gabbro; 8. monzo-gabbro; 9. monzo-diorite; 10. monzonite; 11. quartz monzonite; 12. foidolite; 13. foidmonzo-diorite; 14. foidmonzo-syenite; 15. syenite; 16. foid syenite. Purple area: range of 120–100 Ma granitoid compositions in the Great Xing'an-Songliao Basin in Northeast China.
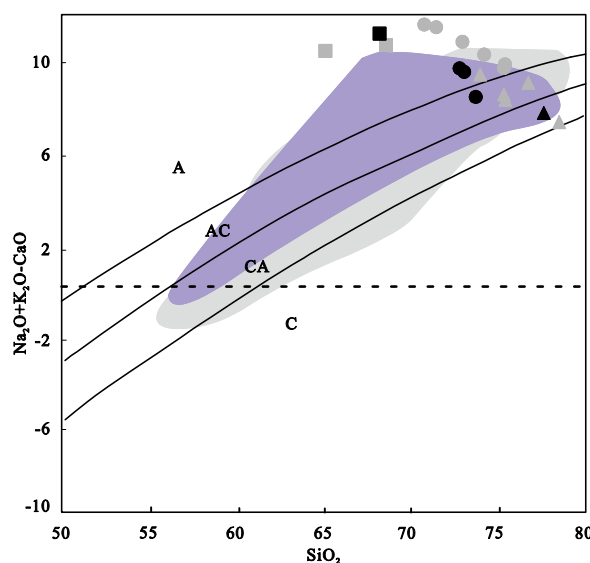
Figure 6. SiO$_2$ versus (Na$_2$O+K$_2$O-CaO) diagram. Black data points are from this study (Table 2), gray data points are from Lin et al. (2003) and Li (1992), colored areas from a dataset of 214 Early Cretaceous granitoid samples from the Great Xing'an-Songliao Basin in northeast China compiled for this paper. Purple area samples formed from 120 to 100 Ma, grey area samples formed from 140 to 120 Ma.

in the age range 120 to 100 Ma (purple area in Figs. 5 and 6).

4.2.2 Trace elements
4.2.2.1 Miarolitic alkaline granite (samples NZS-3–NZS-5)
The trace elements in all samples have broadly similar patterns with elevated Rb, U, Ta, Ce, Nd, and Hf and depleted Ba, K, La, Sr, P, and Ti (Fig. 7b). Contents of Zr+Nb+Ce+Y are from 1 394 ppm to 1 631 ppm, greater than the mean value of the global A-type granite content of 350 ppm proposed by

Table 2 Geochemical compositions of the Nianzishan A-type granitic composite

Sample	NZS-3	NZS-4	NZS-5	NZS-7	NZS-8
Rock type	Alkaline granite			Syenoporphyrite	Rhyolite
SiO_2	72.03	71.98	72.90	67.47	76.25
TiO_2	0.21	0.22	0.22	0.46	0.12
Al_2O_3	13.46	13.46	13.18	16.79	12.84
FeO^T	2.97	2.96	3.39	1.70	0.86
MnO	0.11	0.12	0.14	0.04	0.01
MgO	0.13	0.11	0.10	0.24	0.10
CaO	0.40	0.34	0.21	0.41	0.22
Na_2O	4.88	4.74	5.99	5.50	3.10
K_2O	4.94	5.10	2.53	6.22	4.81
P_2O_5	0.01	0.01	0.01	0.04	n.d.
LOI	0.29	0.36	0.71	0.74	1.37
Total	99.42	99.40	99.38	99.62	99.68
La	104	106	157	51.3	19.2
Ce	209	208	320	122	36.4
Pr	25.2	24.9	39.7	13.6	5.36
Nd	88.1	87.6	128	48.4	19.9
Sm	18.4	17.0	26.4	9.80	6.53
Eu	0.54	0.65	0.72	1.09	0.13
Gd	15.2	13.7	21.1	7.75	7.85
Tb	2.48	2.18	3.56	1.24	1.69
Dy	14.4	12.6	20.1	6.95	11.2
Ho	2.79	2.49	3.89	1.39	2.43
Er	7.88	7.24	10.6	3.86	7.17
Tm	1.18	1.12	1.50	0.58	1.10
Yb	7.71	7.61	9.25	3.69	7.14
Lu	1.19	1.19	1.34	0.57	1.06
Y	77.3	67.5	122.2	38.3	68.2

Sample	NZS-3	NZS-4	NZS-5	NZS-7	NZS-8
Rock type	Alkaline granite			Syenoporphyrite	Rhyolite
∑REE	576	560	867	311	195
LREE	446	444	673	247	87.6
HREE	52.8	48.2	71.4	26.0	39.7
$(La/Yb)_N$	9.14	9.40	11.5	9.38	1.81
Eu/Eu*	0.10	0.13	0.09	0.37	0.06
Sc	3.74	4.32	4.58	7.34	1.48
Ga	29.2	30.3	30.0	28.0	30.2
Rb	164	197	79.7	116	205
Zr	1033	1091	1104	487	825
Nb	73.9	82.6	84.4	48.1	60.6
Mo	1.26	0.89	1.43	0.76	1.10
Cs	0.78	0.87	0.44	1.49	1.47
Hf	21.4	21.1	22.9	9.10	17.2
Ta	4.09	4.78	4.81	2.15	3.60
Pb	38.1	52.2	56.1	19.4	10.8
Th	12.7	14.6	16.3	4.32	15.9
U	2.29	2.77	3.68	0.77	4.71
Ba	62.2	143.0	52.0	194.1	18.3
Cr	3.06	3.12	3.42	3.44	3.68
Sr	6.56	9.63	6.19	17.2	37.4
Zr+Nb+Ce+Y	1393	1449	1631	695	991
10000×Ga/Al	4.10	4.25	4.29	3.14	4.44
Q	23.6	23.8	27.3	10.7	39.7
A	70.6	70.4	63.2	82.0	54.5
P	0.58	0.83	4.14	3.99	2.10
D_{Zr} [①]	480.2	454.3	449.3	1018	600.8
$T_{Zr\ saturation}$ [①] (°C)	962.0	970.4	981.9	877.0	976.8

① $T_{Zr\ saturation}$. The Zr saturation temperature of whole rock; D_{Zr}. the concerntration ratio of Zr in the stoichiometric zircon to that in the melt. The cacultion formula is based on Waston and Harrison (1983).

Whalen et al. (1987). Ratio of 10 000×Ga/Al is >4, which is close to the global average of 3.75 but higher than the boundary value of 2.6 for A-type granites. K/Rb ratios are from 214 to 263, and Rb/Sr are from 12 to 25. The chondrite-normalized REE patterns of the granites are similar (Fig. 7a), exhibiting LREE/HREE fractionation [(La/Yb)$_N$ from 9.14 to 11.46] and negative Eu anomalies (Eu/Eu* from 0.09 to 0.13). Total REE (from 499 ppm to 744 ppm) and heavy REE (from 48.16 ppm to 71.36 ppm) of the studied samples are higher than typical granites. The heavy rare earth elements vary a little perhaps due to fluid-rock interactions. The contents of Rb, Ga, Zr, and Ta in the porphyritic syenite enclosure (sample NZS-7) are high, whereas Ba and U are low. The 10 000×Ga/Al is 3.15. The content of Zr is 486 ppm, and Zr+Nb+Ce+Y is 696 ppm. The chondrite-normalized REE patterns show weak negative Eu anomalies (Eu/Eu*=0.37) and display fractionation of REE similar to the miarolitic alkaline granite [(La/Yb)$_N$=9.38, Fig. 7b]. The rhyolite (sample NZS-8) has contents of Zr, Hf, Nb, Ta, Ga, and Zn enriched; Zr is 825 ppm, K/Rb ratio is 194, and Rb/Sr is 5.5. The contents of Zr+Nb+Ce+Y is 991 ppm and 10 000×Ga/Al is approximately 4. There are obvious negative anomalies in mantle-normalized Ba, Sr, Ti, and P concentrations (Fig. 7b). The total REEs are low (ΣREE=272 ppm). A clear Eu anomaly is observed in the chondrite-normalized REE

diagram, with Eu/Eu*=0.06. However, fractionation of REE is not obvious, and the trend is relatively gentle [La/Yb)$_N$=1.81].

Compared to igneous rocks at 140 to 120 Ma, the NAGC has an extremely high total rare earth content and a more extreme negative Eu anomaly displayed in Fig. 7a. Again, more significant depletion of trace elements (Ba, Sr, Ti, P, Ta, Nb, etc.) can be recognized easily in Fig. 7b.

Zircon saturation temperature (T_{zr}) calculations indicate that temperatures of the NAGC A-type granites are from 961 to 981 ℃, with an average of 971 ℃, whereas T_{zr} values of the enclosure and rhyolite are 875 and 975 ℃. Sui and Chen (2011) obtained T_{zr} values of 868 to 928 ℃ for the NAGC A-type granites. Their T_{zr} values are probably slightly lower than ours because they did not measure $^T Fe_2O_3$. Our calculated T_{zr} value of 971 ℃ should be close to the magma temperature of the A-type granites, and is broadly consistent with temperatures independently constrained by oxygen isotope equilibrium temperatures (Wei et al., 2008).

4.3 Sr and Nd Isotopes

Sr-Nd isotopic data for the NAGC are listed in Table 3. The Sr contents of A-type granites are from 6.19 ppm to 9.63 ppm, compared with 17.20 ppm in the porphyritic syenite. Initial Sr and Nd isotopic ratios were back-corrected using ages of
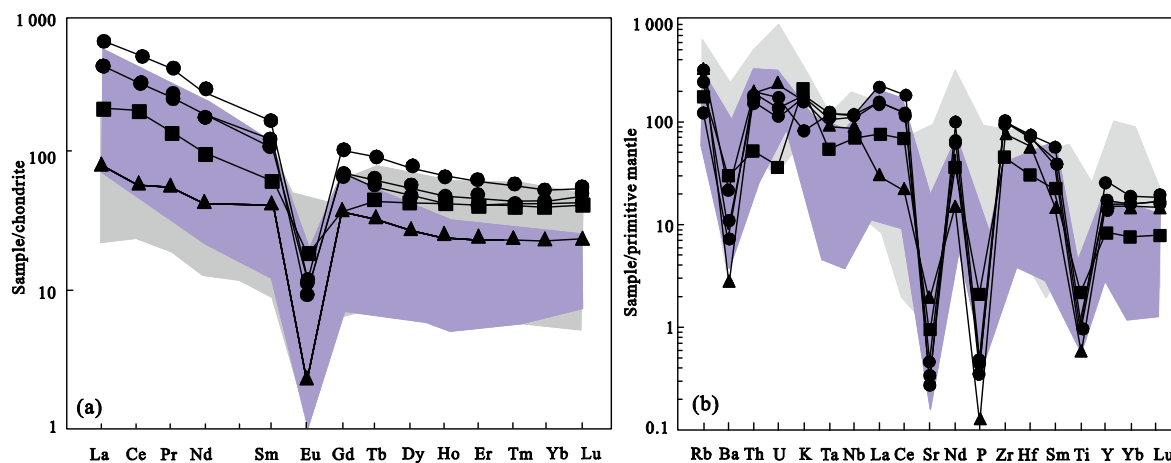
Figure 7. General chondrite normalized rare earth element diagram of the NAGC (Sun and McDonald, 1989).

Table 3 Sr-Nd contents and isotope values

Sample	Rb (ppm)	Sr (ppm)	$^{87}Rb/^{86}Sr$	$^{87}Sr/^{86}Sr$	Sm (ppm)
NZS-3	164.84	6.56	72.746 685	0.714 259	18.41
NZS-4	197.55	9.63	59.381 411	0.712 827	17.02
NZS-7	116.7	17.2	19.644 723	0.715 428	9.8
NZS-8	205.44	37.35	15.916 588	0.710 625	6.53

Sample	Nd (ppm)	$^{147}Sm/^{144}Nd$	$^{143}Nd/^{144}Nd$	$\varepsilon_{Nd}(t)$	T_{DM1}
NZS-3	88.1	0.126 333	0.512 681	1.85	821
NZS-4	87.6	0.117 466	0.512 685	2.06	739
NZS-7	48.39	0.122 407	0.512 678	1.90	791
NZS-8	19.89	0.119 855	0.512 739	1.94	671

112 and 114 Ma for A-type granites, and 118 Ma for porphyritic syenite. Variable and unreasonable ($^{87}Sr/^{86}Sr$)$_0$ ratios less than basaltic achondrite best initial (BABI) (0.698 98) were found due to high $^{87}Rb/^{86}Sr$ ratios. However, the ($^{143}Nd/^{144}Nd$)$_0$ ratios are robust with positive $\varepsilon_{Nd}(t)$ values ranging from +1.85 to +2.06. T_{DM1} ranges from 671 to 821 Ma. The $\varepsilon_{Nd}(t)$ values and T_{DM1} ages for the A-type granite, porphyritic syenite and rhyolite are similar, suggesting a common origin.

5 DISCUSSION

5.1 Timing of Magmatism

Reliable ages of the Nianzishan A-type granitoid complex have been lacking up to now. Li and Yu (1993) obtained an age of 123 Ma for the A-type granites by K-feldspar and biotite Ar-Ar dating, similar to a whole-rock Rb-Sr isochron age obtained by Yan et al. (2000). Li and Yu. (1993) dated porphyritic

syenite at 135 Ma from a whole-rock Rb-Sr isochron. This study has obtained high-precision LA-ICP-MS zircon U-Pb ages of 112.95±0.73 and 114.1±1.7 Ma for the A-type granites and 118.77±0.43 Ma for the porphyritic syenite (Table 4). These newly available ages are younger than those previously reported and suggest that the A-type granites and porphyritic syenite are the products of late stage Early Cretaceous magmatism.

Jahn et al. (2001) reported an Rb-Sr isochron age of 125 Ma for the Baerzhe A-type granite, and Qiu et al. (2014) obtained the same age from zircon U-Pb dating. The Shangmachang A-type granite is 106 Ma old (Wu et al., 2002), and the Alongshan A-type granite crystallized 117 Ma ago. The age of the A-type granite in the Longtoushan is 117 Ma, for the Gangshan A-type granite is 107.7 Ma, and for the Baishilazi A-type granite is 123±3 Ma (Wu et al., 2002), respectively. Qin et al. (2012) reported 117.8 Ma for the Shanglüshuiqiao A-type granite in the Jilin Province. Zhang Q F et al. (2007) and Ge et al. (1999) obtained ages of 111 to 120 and 102 to 107 Ma for volcanics of the Yingcheng Formation (K_{1yc}) at Shenping and Xingcheng, respectively. Nearly 100 igneous samples, of which 10 are A- type granite, are compiled in Fig. 8. There were two main peaks of magmatism during the Period from 140 to 100 Ma. The magmatism between 140 and 120 Ma shows obvious

calc-alkaline affinity and suggests a large-scale tectonic transformation event in the Mesozoic era. But most of the A-type granites occur in the period 120 to 100 Ma.

5.2 Magma Genesis

Nianzishan miarolitic alkaline granite contains sodium-rich pyroxene (aegirine-augite) and arfvedsonite; has high SiO_2, FeO^T, alkalies, K/Na ratios, and FeO^T/MgO ratios; and plots in the alkaline field in Fig. 6. The trace element composition of the Nianzishan miarolitic granite is characteristic of A-type granites. The Nianzishan miarolitic granite is enriched in HFSE (Ga, Zr, Nb, and Y) and REE but depleted in Ba, Sr, P, Ti, and Eu. Zr+Nb+Ce+Y is 1 394 ppm to 1 631 ppm, $\sum$REE is 560.05 ppm to 866.61 ppm, and 10 000×Ga/Al is 4.10–4.29. All these values are much higher than the lowest values usually observed in A-type granites (Whalen et al., 1987). Affinities with A-type granite were evidenced by geological, petrological, mineralogical and geochemical features of the samples studied. Using various discrimination diagrams to further constrain the type of A-type granite, it can be seen that all samples in this study plot into the A-type granite field (Fig. 9). Whole-rock T_{Zr} values suggest that overall magmatic temperatures were higher than 850 ℃ for the NAGC (Table 2), in good agreement with global hot granites (Miller et al., 2003) that originated by low degrees

Table 4 Ages of A-type granites in the Great Xing'an Range-northwestern Songliao Basin in Early Cretaceous

Name	Location	Analytical method	Age	Reference
Alongshan	North of Great Xing'an Range	K-Ar	116–118 Ma	Han et al., 2009
Shangmachang	North of Great Xing'an Range	LA	106 Ma	Wu et al., 2002
Nianzishan	Middle Section of Great Xing'an Range	K-Ar	123 Ma	Li and Yu, 1993
		LA	112, 114 Ma	This study
Baerzhe	Middle Section of Great Xing'an Range	Rb-Sr	122±5 Ma	Jahn et al., 2001
		LA	116–126, 118–127Ma	Qiu et al., 2014
Longtoushan	Zhangguangcai Range	TIMS	117±4 Ma	Liu et al., 2005
Gangshan	Songnen Block	U-Pb	107.7 Ma	Fang, 1989
Baishilazi	Zhangguangcai Range	TIMS	123±3 Ma	Wu et al., 2002
Shanglvshyuiqiao	Zhangguangcai Range	LA	117.8 Ma	Qin et al., 2012
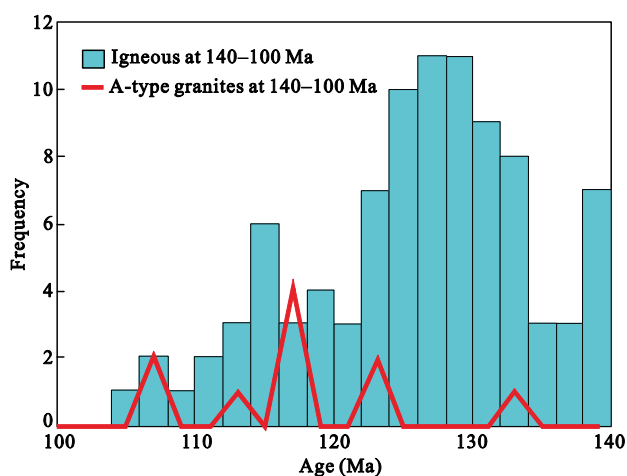
Figure 8. Histogram of age distribution of igneous and A-type granites in the Great Xing'an Range-NE Songliao Basin between 140 to 100 Ma.

of partial melting of dry source rock(s) by dehydration reactions in extensional settings (e.g., Creaser et al., 1991; Clement et al., 1986).

5.3 Magma Source

Whole-rock Sr-Nd isotope data for the Nianzishan A-type granite have previously been published (Wei et al., 2002, 2001a, b; Li and Yu, 1993; Li, 1992), but because of low Sr contents and high $^{87}Rb/^{86}Sr$ ratios, there were large uncertainties in back-corrected $(^{87}Sr/^{86}Sr)_0$ ratios (Wu et al., 1999; Li, 1992).

Such previous studies in NE China reported positive $\varepsilon_{Nd}(t)$ values, low $(^{87}Sr/^{86}Sr)_0$, and young T_{DM1} (Li J Y et al., 2014; Li H X et al., 2012; Guo et al., 2010; Zhang J H et al., 2008; Liu et al., 2005; Lin et al., 2003; Jahn et al., 2001; Shao et al,. 1999). The high $\varepsilon_{Nd}(t)$ and low $(^{87}Sr/^{86}Sr)_0$ ratios for granites from the west coast of the United States have been used to constrain mantle material input into the continental margin, but

mantle input cannot explain the isotopic distribution of igneous rocks in Northeast China. Wu et al. (1999) and Hong et al. (2000) suggested that the positive $\varepsilon_{Nd}(t)$ and low initial I_{Sr} ratios from the Xing'an-Mongolian orogenic belt in NE China might represent new underplating material derived from partial melting of subducted oceanic crust.

As shown in Fig. 10, all samples from the Xing'an-Mongolian orogenic belt plot between CHUR and DM lines. Hong et al. (2000) suggested that the T_{DM1} ages of the granites in the Xing'an-Mongolian orogenic belt coincided with the expansion of the Paleo-Asian Ocean during the Proterozoic, and the granites were derived from partial melting of subducted oceanic crust. Combined whole-rock Nd and zircon oxygen isotopes (low $\delta^{18}O$ values ranging from 3.08‰ to 4.27‰ for non-metamict phases) further indicated that gabbroic oceanic

crust could be the source rock of the Nianzishan A-type granites, and their formation contributed to the net continental growth during the Late Mesozoic (Wei et al., 2008, 2002, 2001a, b).

5.4 Geological Implications
5.4.1 Tectonic setting

A-type granites were once thought to be rifting related, e.g., in Nigeria and Greenland. However, subsequent studies showed that A-type granites also occur within post-orogenic settings (Eby, 1992). The tectonic setting of the NAGC is therefore constrained by major and trace elements in this study. It can be seen that all available samples fall clearly within the A_1-type field (Figs. 11a, 11b, 11c) and the AA field (Fig. 11d) (Hong et al., 1995). Both AA and A_1 represent extensional settings. On the tectonic discrimination diagrams of Pearce
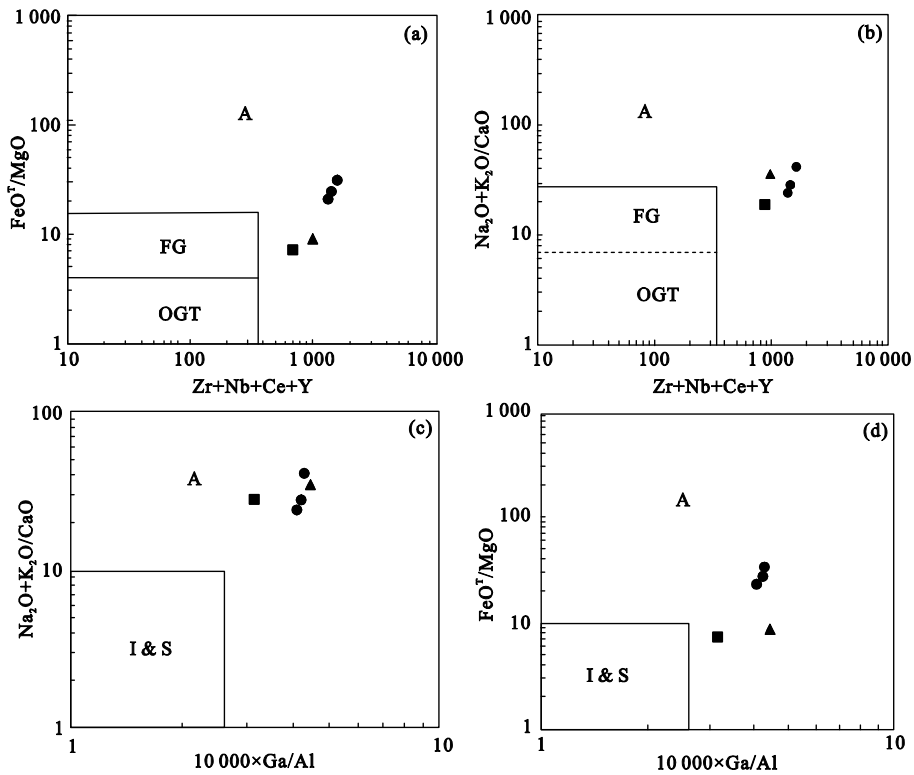
Figure 9. Discrimination diagrams for A-type granites. (a) FeO^T/MgO versus $Zr+Nb+Ce+Y$; (b) Na_2O+K_2O/CaO versus $Zr+Nb+Ce+Y$; (c) Na_2O+K_2O/CaO versus $10\,000\times Ga/Al$; (d) FeO^T/MgO versus $10\,000\times Ga/Al$ (after Whalen et al., 1987).
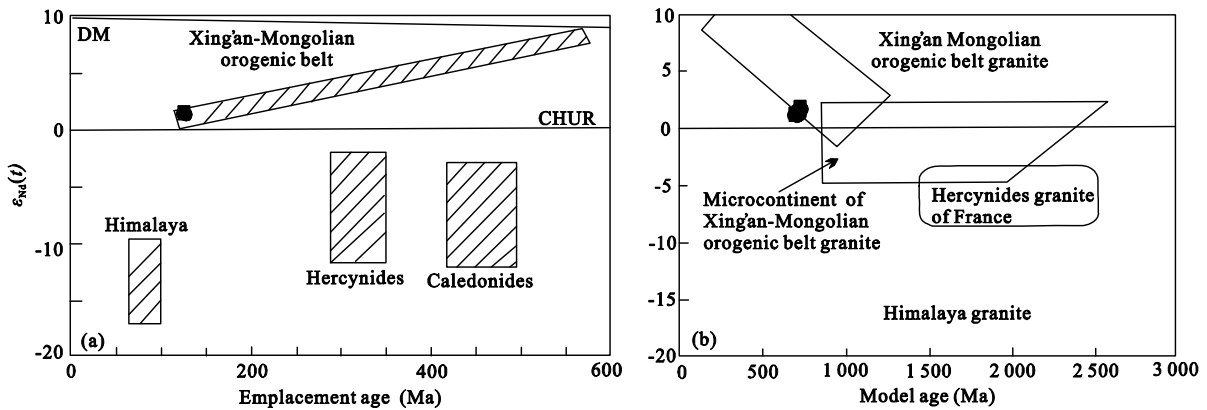
Figure 10. $\varepsilon_{Nd}(t)$ versus emplacement age and $\varepsilon_{Nd}(t)$ versus model age (T_{DM1}) (b) diagrams (after Hong et al., 2000).

(1984), samples from the NAGC plot in within plate environments (WPG in Fig. 12).

5.4.2 Petrotectonic assemblage

The notion of petrotectonic assemblages was first proposed by Dickinson (1971) to identify ancient tectonic settings (Condie, 2014). The concept reflects a correlation between igneous rocks and tectonic environment (Deng et al., 2007, 2004, 1996).

The NAGC is located on the east side of the XMOB at the junction of the Xing'an and Songnen blocks. In this area Early Cretaceous (140 to 120 Ma) intrusive rocks comprise alkalifeldspar granite, granite, quartz monzonite, granodiorite, tonalite, monzonite, and melteigite (Table 5). The Peacock index results show that they mainly comprise CA and only a small amount of calcium (C) and AC. Exposed intrusive rocks are less common in the later part of the Early Cretaceous (120–100 Ma) and comprise alkali granite, syenogranite, granite, porphyry, diorite, and metamorphic core complexes. Intrusive rocks are predominantly alkaline (A) and AC. The Mesozoic granitoids of Jilin Province are granite and monzonitic granite (CA) at 130 to 120 Ma and alkali-feldspar granite composites (A) at 115 Ma (Sui, 1995).
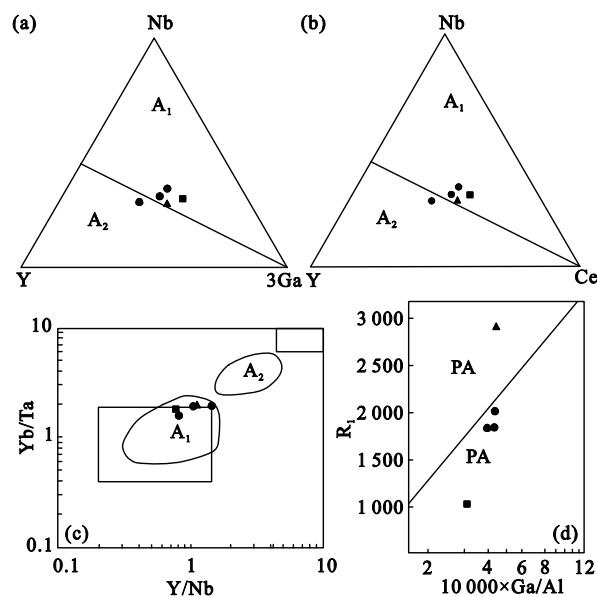
Figure 11. (a) and (b) Nb-Y-3Ga and Nb-Y-Ce triangles (after Eby, 1992); (c) Yb/Ta versus Y/Nb diagram (after Eby, 1992); (d) R_1 versus 10 000×Ga/Al diagram (after Hong et al., 2000).
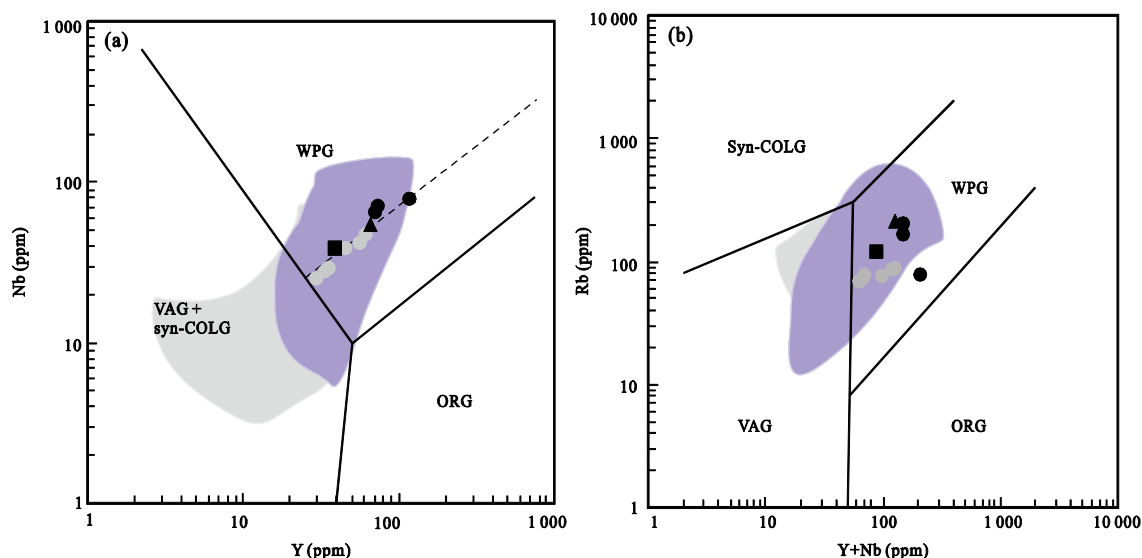
Figure 12. Tectonic discrimination diagrams for the NAGC (after Pearce et al. 1984). Solid data points are from this study, gray ones are after Lin et al. (2003).

Table 5 Petrotectonic assemblage of the Great Xing'an Range-Songliao Basin in Early Cretaceous

Epoch	Intrusive assemblage	References
140–120 Ma (K_{1-1})	Alkali-feldspar granite-granite-quartz monzonite-granodiorite-tonalite-monzonite-melteigite	Qin et al., 2019; She et al., 2012; Wu et al., 2009; Sui, 1995
120–100 Ma (K_{1-2})	Alkali granite-syenogranite-granite prophyry-sillite-dioritic porphyrite-metamorphic core complex	Wang et al., 2013; Guo et al., 2012; Liu C et al., 2011; Sun et al., 2008; Cheng et al., 2006; Liu W et al., 2005; Lin et al., 2004; Wu et al., 2002; Zhang and Shao, 1998; Wang and Zhao, 1997; Li and Yu, 1993

Epoch	Volcanic assemblage	References
140–120 Ma (K_{1-1})	Olive basaltic-andesite-mugearite-gibelite-latite-trachyte-olivine basalt-rhyolite	Zhao et al., 2013; Meng et al., 2011; Zhang, 2009; Zhang Y T et al., 2007
120–100 Ma (K_{1-2})	Rhyolite-comendite-dacite-andesite-trachyandesite-basalt (bimodal volcanic rock)	Wang et al., 2015; Liu R P et al., 2015; Meng et al., 2014; Liu W et al., 2014; Jin, 2012; Xu et al., 2010; Zhang, 2009; Dong et al., 2008; Lin et al., 2003

Volcanic rocks outcrop in the Great Xing'an Range and the western Songliao Basin and range stratigraphically from old to new as follows: Shangkuli Formation (K$_1$s), Illek Group (K$_1$y), Mailer Group (K$_1$m), and Baiyingaolao Group (K$_1$b). The Early Cretaceous (140 to 120 Ma) volcanics are olivine basaltic andesite, mugearite, latite, trachyte, olivine basalt, and rhyolite. Rocks show CA and AC properties, and the olivine basalts are tholeiitic (TH).

Volcanic assemblages at 120 to 100 Ma are composed of rhyolite, alkaline rhyolite, anganite, andesite, and basalt and occur in the Yingcheng Group (K$_{1yc}$) in the Songliao Basin. The volcanics are mainly alkaline (A). Rhyolite in the margin of the Songliao Basin exhibits A-type characteristics (Wang and Xu, 2003; Ge et al., 2000). The rhyolitic cover of the NAGC has A-type characteristics, and its age and geochemistry are consistent with the volcanics of the Yingcheng Group (K$_{1yc}$) (Liu et al., 2014; Li and Yu, 1993).

These igneous rocks suggest an active continental margin and arc environment in the Great Xing'an Range and Songliao Basin during the Early Cretaceous (K$_{1-1}$) and the Ergun Block suggests an extensional setting. The igneous assemblages for the later part of the Early Cretaceous (K$_{1-2}$) all suggest stretching and thinning.

5.4.3 Timing constrains on regional extension

Wang and Xu (2003) studied the formation pressure of Mesozoic volcanic rocks in the Songliao Basin and proposed that basaltic trachyandesite and trachyandensite of the Huoshiling Group formed at 1.0 to 1.2 GPa. The Shahezi Group and Illek Group in the Great Xing'an Range yielded pressures of 1.2 to 1.4 GPa, and the Yincheng Group formed at 0.6 to 1.0 GPa. Differences in pressure suggest that the lithospheric thickness varied from 40 to 20 km and 46 to 90 km and was the thinnest (20 to 30 km) at 120 to 100 Ma.

In summary, igneous rocks related to compressional settings were widespread in the Great Xing'an Range-Songliao Basin at 140 to 120 Ma, and roots of the lithosphere from that period still exist (Fig. 13a). With continuing subduction of the Paleo-Pacific Plate, large scale delamination occurred in the NE China and the lithospheric thinning reached its peak from 120 to 100 Ma (Fig. 13b).
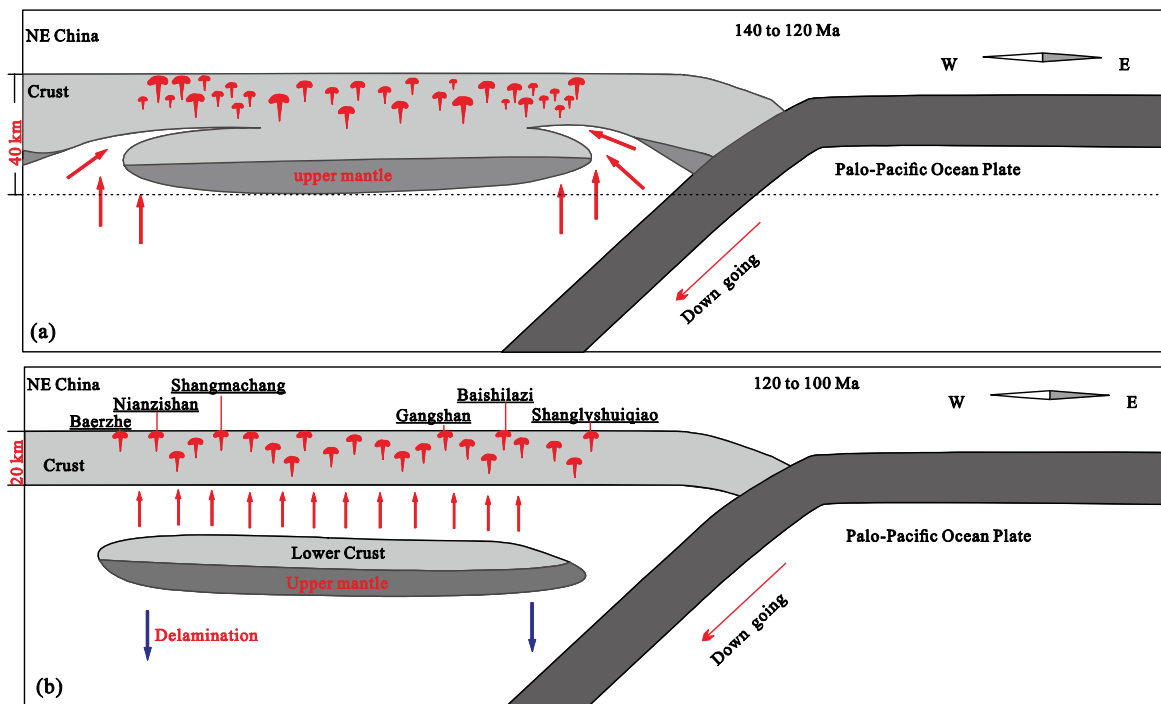
Figure 13. Tectonic evolution model of northeast China at 140 to 120 Ma. (a) Period of 140 to 120 Ma, transition stage from compressed to extended setting with lithospheric roots still there. (b) Period of 120 to 100 Ma, peak stage of lithospheric delamination and thinning (Lithospheric thickness data from Wang and Xu, 2003).

6   CONCLUSIONS

(1) The age of the Nianzishan A-type granite is from 112.95±0.93 to 114.1±1.7 Ma, and the age of the porphritic syenite is 118.6±0.51 Ma. Sr-Nd isotopes and Nd model ages suggest that they originated from partial melting of a common juvenile crust source rock.

(2) The geochemical characteristics of the Nianzishan A-type granitoid complex suggest an affinity with A$_1$- or AA-subtype granite formed within an extensional setting.

(3) The occurrence of the NAGC suggests that the Great Xing'an Range-Songliao Basin underwent lithosphere thinning and extension from 120 to 100 Ma.

REFERENCES CITED

Bonin, B., 2007. A-Type Granites and Related Rocks: Evolution of a Concept, Problems and Prospects. *Lithos*, 97(1/2): 1–29. https://doi.org/10.1016/j.lithos.2006.12.007

Cheng, R. Y., Wu, F. Y., Ge, W. C., et al., 2006. Emplacement Age of the Raohe Complex in Eastern Heilongjiang Province and the Tectonic Evolution of the Eastern Part of Northeastern China. *Acta Petrologica Sinica*, 22: 353–376. https://doi.org/10.3321/j.issn:1000-0569.2006.02.009 (in Chinese with English Abstract)

Clement, J. D., Holloway, J. R., White, A. J. R., 1986. Origin of A Type Granites: Experimental Constraints. *Am. Mineral*, 71: 317–324

Collins, W. J., Beams, S. D., White, A. J. R., et al., 1982. Nature and Origin of A-Type Granites with Particular Reference to Southeastern Australia. *Contributions to Mineralogy and Petrology*, 80(2): 189–200. https://doi.org/10.1007/bf00374895

Condie, K. C., 2014. Growth of Continental Crust: A Balance between Preservation and Recycling. *Mineralogical Magazine*, 78(3): 623–637. https://doi.org/10.1180/minmag.2014.078.3.11

Creaser, R. A., Price, R. C., Wormald, R. J., 1991. A-Type Granites Revisited: Assessment of a Residual-Source Model. *Geology*, 19(2): 163–166. https://doi.org/10.1130/0091-7613(1991)019<0163:atgrao>2.3.co;2

Deng, J. F., Luo, Z. H., Su, S. G., et al., 2004. Rock Formation Tectonic Environment and Mineralization. Geological Publishing House, Beijng. 1–381 (in Chinese)

Deng, J. F., Xiao, Q. H., Su, S. G., et al., 2007. Igneous Petrotectonic Assemblages and Tectonic Settings: A Discussion. *Geological Journal of China Universities*, 13: 392–402

Deng, J. F., Zhao, H. L., Mo, X. X., et al., 1996. Continent Roots-Plume Tectonic of China-Key to the Continental Dynamics. Geological Publishing House, Beijng. 1–100 (in Chinese)

Dickinson, W. R., 1971. Plate Tectonics in Geologic History. *Science*, 174(4005): 107–113. https://doi.org/10.1126/science.174.4005.107

Dong, S. Y., Yang, T. Z., Zhang, Z. C., 2008. Chronology, Geochemistry and Tectonic Background of Mesozoic Volcanic Rocks in Little Xing'an Range Area. *Bulletin of Mineralogy Petrology and Geochemistry*, 27(Z1): 245–257. https://doi.org/10.3969/j.issn.1007-2802.2008.z1.136 (in Chinese with English Abstract)

Eby, G. N., 1990. The A-Type Granitoids: A Review of Their Occurrence and Chemical Characteristics and Speculations on Their Petrogenesis. *Lithos*, 26(1/2): 115–134. https://doi.org/10.1016/0024-4937(90)90043-z

Eby, G. N., 1992. Chemical Subdivision of the A-Type Granitoids: Petrogenetic and Tectonic Implications. *Geology*, 20(7): 641. https://doi.org/10.1130/0091-7613(1992)020<0641:csotat>2.3.co;2

Fang, W. C. 1989. Granitiod and Minerogenesis of Jilin Province. Jilin Science and Technology Press, Changchun. 9–16 (in Chinese with English Abstract)

Frost, C. D., Ramo, O. T. and Dallagnol, R., 2007. IGCP Project 510—A-Type Granites and Related Rocks through Time. *Lithos*, 97(1/2): vii–xiii. https://doi.org/10.1016/j.lithos.2007.01.006

Ge, W. C., Lin, Q., Sun, D. Y., et al., 1999. Geochemical Characteristics of the Mesozoic Basalts in Da Hinggan Ling: Evidence of the Mantle Crust Interaction. *Acta Petrologica Sinica*, 15: 397–407. https://doi.org/10.3321/j.issn:1000-0569.1999.03.008 (in Chinese with English Abstract)

Ge, W. C., Lin, Q., Sun, D. Y., et al., 2000. Geochemical Research into Origins of Two Types of Mesozoic Rhyolites in Daxing'anling. *Earth Science—Journal of China University of Geosciences*, 25: 172–178. https://doi.org/10.3321/j.issn:1000-2383.2000.02.012 (in Chinese with English Abstract)

Guo, F., Fan, W. M., Gao, X. F., et al., 2010. Sr-Nd-Pb Isotope Mapping of Mesozoic Igneous Rocks in NE China: Constraints on Tectonic Framework and Phanerozoic Crustal Growth. *Lithos*, 120(3/4): 563–578. https://doi.org/10.1016/j.lithos.2010.09.020

Guo, J., Huang, Y. W., Sun, J. G., et al., 2012. Zircon LA-ICP-MS U-Pb Dating of Giorite-Porphyrite from Sishanlinchang Gold Deposit in Heilongjiang and Its Geological Significance. *Global Geology*, 31: 20–27. https://doi.org/10.1007/s11783-011-0280-z (in Chinese with English Abstract)

Han, Z. Z., Wang, H. J., Zhong, H. L., et al., 2009. Geochemical Characteristics and Tectonic Significance of Early Cretaceous A-Type Granite in Alongshan Area, Northeastern Inner Mongolia. *Geology and Mineral Resources of South China*, 4: 1–9. https://doi.org/10.3969/j.issn.1007-3701.2009.04.001 (in Chinese with English Abstract)

Hong, D. W., Wang, S. G., Han, B. F., et al., 1995. The Tectonic Setting of the Alkali Granite Classification and Its Identification Marks. *Science in China*: *Series B*, 25: 418–426. https://doi.org/10.1007/BF02657001 (in Chinese with English Abstract)

Hong, D. W., Wang, S. G., Xie, X. L., 2000. Genesis of Positive $\varepsilon_{Nd}(t)$ Granitoids in the Da Hinggan Mts.-Mongolia-Orogenic Belt and Growth Continental Crust. *Earth Science Frontiers*, 7: 441–456. https://doi.org/10.3321/j.issn:1005-2321.2000.02.012 (in Chinese with English Abstract)

Jahn, B. M., Wu, F. Y., Capdevila, R., et al., 2001. Highly Evolved Juvenile Granites with Tetrad REE Patterns: The Woduhe and Baerzhe Granites from the Great Xing'an Mountains in NE China. *Lithos*, 59(4): 171–198. https://doi.org/10.1016/s0024-4937(01)00066-4

Jin, X., 2012. Zircon U-Pb Ages and Zircon Hf Isotopic Composition of Volcanic Rocks in the Northern Songliao Basin: [Dissertation]. Jinlin University, Changchun (in Chinese with English Abstract)

King, P. L., White, A. J. R., Chappell, B. W., et al., 1997. Characterization and Origin of Aluminous A-Type Granites from the Lachlan Fold Belt, Southeastern Australia. *Journal of Petrology*, 38(3): 371–391. https://doi.org/10.1093/petroj/38.3.371

Leake, B. E., Woolley, A. R., Arps, C. E. S., et al., 1997. Nomenclature of Amphiboles: Report of the Subcommittee on Amphiboles of the International Mineralogical Association, Commission on New Minerals and Mineral Names. *European Journal of Mineralogy*, 9(3): 623–651. https://doi.org/10.1127/ejm/9/3/0623

Li, H. X., Guo, F., Li, C. W., et al., 2012. Petrogenesis of Early Cretaceous Tonalites from the Xiaoxinancha Au-Cu Deposit. *Geochemistry*, 41: 497–514. https://doi.org/10.1007/s11783-011-0280-z (in Chinese with English Abstract)

Li, J. Y., Guo, F., Li, C. W., et al., 2014. Neodymium Isotopic Variations of Late Paleozoic to Mesozoic I- and A-Type Granitoids in NE China: Implications for Tectonic Evolution. *Acta Petrologica Sinica*, 30:

1995–2008. https://doi.org/10.1016/j.pgeola.2014.02.004 (in Chinese with English Abstract)

Li, P. Z., 1992. The Relationship between δD and Magma Degassing of the Nianzishan Miarolitic Alkaline Granite Heilongjiang. *Geochemisry*, 4: 70–76. https://doi.org/10.19700/j.0379-1726.1992.01.00 (in Chinese with English Abstract)

Li, P. Z., Yu, J. S., 1993. Nianzishan Miarolitic Alkaline Granite Stock, Heilongjiang—Its Ages and Geological Implications. *Geochemica*, 22: 389–399. https://doi.org/10.19700/j.0379-1726.1993.04.009 (in Chinese with English Abstract)

Lin, Q., Ge, W. C., Cao, L., et al., 2003. Geochemistry of Mesozoic Volcanic Rocks in Da Hinggan Ling: The Bimodal Volcanic Rocks. *Geochemica*, 32: 208–222. https://doi.org/10.3321/j.issn:0379-1726.2003.03.002 (in Chinese with English Abstract)

Lin, Q., Ge, W. C., Wu, F. Y., et al., 2004. Geochemistry of Mesozoic Granites in Da Hinggan Ling Ranges. *Acta Petrologica Sinica*, 20: 403–412. https://doi.org/10.1007/BF02873097 (in Chinese with English Abstract)

Liu, C. S., Chen, X. M., Chen, P. R., et al., 2003. Subdivision, Discrimination Criteria and Genesis for A Type Rocks Suites. *Geological Journal of China Universities*, 9: 573–591. https://doi.org/10.1016/S0955-2219 (02)00073-0 (in Chinese with English Abstract)

Liu, C., Deng, J. F., Xu, L. Q., et al., 2011. A Preliminary Frame of Magma-Tectonic Mo Metallogenic Events of Mesozoic Era in Da Hinggan Mountains and Xiao Hinggan Mountains Areas. *Earth Science Frontiers*, 18: 166–178. https://doi.org/10.1007/s12182-011-0118-0 (in Chinese with English Abstract)

Liu, R. P., Gu, X. X., Zhang, Y. M., et al., 2015. Zircon U-Pb Geochronology Petrogeochemistry of Host Ignous Rocks of the Dong'an Gold Deposit in Heillongjiang Province, NE China, *Aacta Petrologica Sinica*, 31: 1391–1408. https://doi.org/10.3969/j.issn.1007-2802.2014.05.011 (in Chinese with English Abstract)

Liu, W., Siebel, W., Li, X. J., et al., 2005. Petrogenesis of the Linxi Granitoids, Northern Inner Mongolia of China: Constraints on Basaltic Underplating. *Chemical Geology*, 219(1/2/3/4): 5–35. https://doi.org/10.1016/j.chemgeo.2005.01.013

Liu, W., Sun, D. Y., Li, R. L., 2014. Chronology and Petrogenesis of Volcanic Rocks in Yingcheng Formation from Changling Depression in Songliao Basin: [Dissertation]. Jilin University, Changchun (in Chinese with English Abstract)

Loiselle, M. C., Wones, D. R., 1979. Characteristics and Origin of Anorogenic Granites. *Geol. Soc. Am. Prog.* (*Abstracts with Programs*), 11: 468

Ludwig. K, R., 2003. Isoplot/Ex, a Geochronological Toolkit for Microsoft Excel, Version 3.00. Berkeley Geochronology Center, Berkeley

Meng, F. C., Liu, J. Q., Cui, Y., et al., 2014. Mesozoic Tectonic Regimes Transition in the Northeast China: Constriants from Temporal-Spatial Distribution and Association of Volcanic Rocks. *Acta Petrologica Sinica*, 30: 3569–3586 (in Chinese with English Abstract)

Meng, G., Xu, W. L., Yang, D. B., 2011. Zircon U-Pb Chronology, Geochemistry of Mesozoic Volcanic Rocks from the Lingquan Basin in Manzhouli Area, and Its Tectonic Implications. *Acta Petrologica Sinica*, 27: 1209–1226 (in Chinese with English Abstract)

Middlemost, E. A. K., 1994. Naming Materials in the Magma/Igneous Rock System. *Earth-Science Reviews*, 37(3/4): 215–224. https://doi.org/10.1016/0012-8252(94)90029-9

Miller, C. F., McDowell, S. M., Mapes, R. W., 2003. Hot and Cold Granites? Implications of Zircon Saturation Temperatures and Preservation of Inheritance. *Geology*, 31(6): 529–532.

https://doi.org/10.1130/0091-7613(2003)031<0529:hacgio>2.0.co;2

Morimoto, N., 1988. Nomenclature of Pyroxenes. *Mineralogy and Petrology*, 39: 55–76. https://doi.org/10.1007/bf01226262

Nasdala, L., Hofmeister, W., Norberg, N., et al., 2008. Zircon M257—A Homogeneous Natural Reference Material for the Ion Microprobe U-Pb Analysis of Zircon. *Geostandards and Geoanalytical Research*, 32(3): 247–265. https://doi.org/10.1111/j.1751-908x.2008.00914.x

Norrish, K., Chappell, B. W., 1977. X-Ray Fluorescence Spectrometry. In: Zussman, J., ed., Physical Methods in Determinative Mineralogy: 2nd ed. Academic Press, London. 201–272

Pearce, J. A., Harris, N. B. W., Tindle, A. G., 1984. Trace Element Discrimination Diagrams for the Tectonic Interpretation of Granitic Rocks. *Journal of Petrology*, 25(4): 956–983. https://doi.org/10.1093/petrology/25.4.956

Qi, L., Hu, J., Gregoire, D. C., 2000. Determination of Trace Elements in Granites by Inductively Coupled Plasma Mass Spectrometry. *Talanta*, 51(3): 507–513. https://doi.org/10.1016/s0039-9140(99)00318-5

Qian, C., Lu, L., Qin, T., et al., 2018. A Study of the Late Pleistocene Action of Yaluhe fault in Northern DaHinggan Mountains. *Geological Bulletin of China*, 37(9): 1748–1754. https://doi.org/cnki:sun:zqyd.0.2018-09-021 (in Chinese with English Abstract)

Qiao, G. S., 1988. Normalization of Isotopic Dilution Analysis—A New Program for Isotope Mass Spectrometric Analysis. *Science in China*: *Series A*, 31: 1263–1268 (in Chinese with English Abstract)

Qin, J. H., Liu, C., Shi, Y. R., et al., 2019. Formation Age, Characteristics and Geological Significance of Boketu Miarolitic Granite in Inner Mongolia. *Earth Science*, 44(4): 1295–1310. https://doi.org/10.3799/dqkx.2018.585 (in Chinese with English Abstract)

Qin, Y., Liang, Y. H., Hu, Z. C., et al., 2012. Geochemical Characteristics and Tectonic Significance of the Shanglvshuqiao Aluminous A-Type Granite Instrusive in the Ji'an Area, Jilin Province. *Journal of Jilin University*: *Earth Science Edition*, 1076–1083. https://doi.org/10.13278/j.cnki.jjuese.2012.04.034 (in Chinese with English Abstract)

Qiu, Z. L., Liang, D. Y., Wang, Y. F., 2014. Zircon REE, Trace Element Characteristics and U-Pb Chonology in the Baerzhe Alkaline Granite: Implications to the Petrological and Mineralization. *Acta Petrologica Sinica*, 30: 1757–1768 (in Chinese with English Abstract)

Rubatto, D., 2002. Zircon Trace Element Geochemistry: Partitioning with Garnet and the Link between U-Pb Ages and Metamorphism. *Chemical Geology*, 184(1/2): 123–138. https://doi.org/10.1016/s0009-2541(01)00355-2

Schulz, B., Klemd, R., Brätz, H., 2006. Host Rock Compositional Controls on Zircon Trace Element Signatures in Metabasites from the Austroalpine Basement. *Geochimica et Cosmochimica Acta*, 70(3): 697–710. https://doi.org/10.1016/j.gca.2005.10.001

Şengör, A. M. C., Natal'in, B. A., 1996. Paleotectonics in Asia: Fragments of a Synthesis. In: Yin, A., ed., The Tectonic Evolution of Asia. Cambridge University Press, Cambridge. 486–640

Şengör, A. M. C., Natal'in, B. A., Burtman, V. S., 1993. Evolution of the Altaid Tectonic Collage and Palaeozoic Crustal Growth in Eurasia. *Nature*, 364(6435): 299–307. https://doi.org/10.1038/364299a0

Shao, J. A, Zhang, L. Q., Mu, B. L., 1999. Magatism in the Mesozoic Extending Orogenic Process of Dahinggan MTS. *Earth Science Frontiers*, 6: 339–346. https://doi.org/10.3321/j.issn:1005-2321.1999.04.017 (in Chinese with English Abstract)

She, H. Q., Li, J. W., Xiang, A. P., et al., 2012. U-Pb Ages of the Zircons from Primary Rocks in Middle-Northern Daxinganling and Its Implica-

tions to Geotectonic Evolution. *Acta Petrologica Sinica*, 28: 571–594 (in Chinese with English Abstract)

Sláma, J., Košler, J., Condon, D. J., et al., 2008. Plešovice Zircon—A New Natural Reference Material for U-Pb and Hf Isotopic Microanalysis. *Chemical Geology*, 249(1/2): 1–35. https://doi.org/10.1016/j.chemgeo.2007.11.005

Sui, Z. M., 1995. The Genesis of Mesozoic Granites in Jilin Province and Its Tectonic Setting. *Jilin Geology*, 1: 15–22 (in Chinese with English Abstract)

Sui, Z. M., Chen, Y. J., 2011. Zircon Saturation Temperatures of Granites in Eastern Great Xing'an Range, and Its Geological Signification. *Global Geology*, 30: 162–172. https://doi.org/10.1007/s11589-011-0776-4 (in Chinese with English Abstract)

Sun, J. G., Chen, L., Zhao, J. K., 2008. SHRIMP U-Pb Dating of Zircon from Late Yanshanian Granitic Complex in Xiaoxinancha Gold-Rich Copper Orefield of Yanbian and Its Geological Implications. *Mineral Deposits*, 27: 319–328. https://doi.org/10.1002/clen.200700058 (in Chinese with English Abstract)

Sun, S. S., McDonough, W. F., 1989. Chemical and Isotopic Systematics of Oceanic Basalts: Implications for Mantle Composition and Processes. *Geological Society*, *London*, *Special Publications*, 42(1): 313–345. https://doi.org/10.1144/gsl.sp.1989.042.01.19

Tian, D. X., Ge, W. C., Yang, H., et al., 2014. Lower Cretaceous Alkali Feldspar Granites in the Central Part of the Great Xing'an Range, Northeastern China: Chronology, Geochemistry and Tectonic Implications. *Geological Magazine*, 152(3): 383–399. https://doi.org/10.1017/s0016756814000387

Wang, H. Q, Xu, W. L., 2003. The Deep Process of Formation and Evolution of Songliao Basin: Mesozoic Vocanic Rock Probe. *Journal of Jilin University*: *Earth Sicence Eidition*, 33: 37–42. https://doi.org/10.3969/j.issn.1671-5888.2003.01.007 (in Chinese with English Abstract)

Wang, L. G., Han, Y. P., Chai, P., 2013. Zircon U-Pb Dating of Diorite Breccias from J_0 Ore Body in Jinchang Gold Deposit of Heilongjiang and Its Geological Significance. *Global Geology*, 32: 515–521. https://doi.org/10.3969/j.issn.1004-5589.2013.03.008 (in Chinese with English Abstract)

Wang, Q. S., Yang, Y. C., Han, S. J., et al., 2015. Geochemical Characteristics and LA-ICP-MS Zircon U-Pb Dating of Xianfengbeishan Gold Deposite in Heilongjiang Province and Their Geological Significance. *Mineral Deposits*, 34: 675–691. https://doi.org/10.16111/j.0258-7106.2015.04.002 (in Chinese with English Abstract)

Wang, Y. X., Zhao, Z. H., 1997. Geochemistery and Origin of the Baerzhe REE-Nb-Be-Zr Superlarge Deposit. *Geochemica*, 26: 24–35. https://doi.org/10.3969/j.issn.1000-6524.2000.04.002 (in Chinese with English Abstract)

Watson, E. B., Harrison, T. M., 1983. Zircon Saturation Revisited: Temperature and Composition Affects in a Variety of Crustal Magma Types. *Earth and Planetary Science Letters*, 64(2): 295–304. https://doi.org/10.1016/0012-821x(83)90211-x

Wei, C. S., Zhao, Z. F., Spicuzza, M. J., 2008. Zircon Oxygen Isotopic Constraint on the Sources of Late Mesozoic A-Type Granites in Eastern China. *Chemical Geology*, 250(1/2/3/4): 1–15. https://doi.org/10.1016/j.chemgeo.2008.01.004

Wei, C. S., Zheng, Y. F., Zhao, Z. F., 2001a. Nd-Sr-O Isotopic Geochemistry Constraints on the Age and Origin of the A-type Granites in Eastern China. *Acta Petrologica Sinica*, 17: 95–111.

https://doi.org/10.3969/j.issn.1000-0569.2001.01.010 (in Chinese with English Abstract)

Wei, C. S., Zheng, Y. F., Zhao, Z. F., et al., 2001b. Oxygen Isotope Evidences of Two-Stage Water-Rock Interaction in Nianzishan A-Type Granite. *Chinese Science Bulletin*, 46: 8–13. https://doi.org/10.3321/j.issn:0023-074X.2001.01.002 (in Chinese with English Abstract)

Wei, C. S., Zheng, Y. F., Zhao, Z. F., et al., 2002. Oxygen and Neodymium Isotope Evidence for Recycling of Juvenile Crust in Northeast China. *Geology*, 30(4): 375. https://doi.org/10.1130/0091-7613(2002)030 <0375:oanief>2.0.co;2

Whalen, J. B., Currie, K. L., Chappell, B. W., 1987. A-Type Granites: Geochemical Characteristics, Discrimination and Petrogenesis. *Contributions to Mineralogy and Petrology*, 95(4): 407–419. https://doi.org/10.1007/bf00402202

Wu, F. Y., Sun, D. Y., Ge, W. C., et al., 2011. Geochronology of the Phanerozoic Granitoids in Northeastern China. *Journal of Asian Earth Sciences*, 41(1): 1–30. https://doi.org/10.1016/j.jseaes.2010.11.014

Wu, F. Y., Sun, D. Y., Li, H. M., et al., 2002. A-Type Granites in Northeastern China: Age and Geochemical Constraints on Their Petrogenesis. *Chemical Geology*, 187(1/2): 143–173. https://doi.org/10.1016/s0009-2541(02)00018-9

Wu, F. Y., Sun, D. Y., Lin, Q., 1999. Petrogenesis of the Phanerozoic Granites and Crustal Growth in Northeast China. *Acta Petrologica Sinica*, 15: 181–189. https://doi.org/10.3321/j.issn:1000-0569.1999.02.003 (in Chinese with English Abstract)

Wu, G., Chen, Y. J., Zhao, Z. H., 2009. Geochemistry, Zircon SHRIMP U-Pb Age and Petrogenesis of the East Luoguhe Granites at the Northern End of the Great Hinggan Range. *Acta Petrologica Sinica*, 25: 233–247 (in Chinese with English Abstract)

Wu, Y. B., Zhen, Y. F., 2004. Study on Zirconium Gallstone by Mineralogy and Its Restriction on U-Pb Age Explanation. *Chinese Science Bulletin*, 49: 1589–1604. https://doi.org/10.1360/csb2004-49-16-1589 (in Chinese with English Abstract)

Xu, W. L., Wang, F., Pei, F. P., et al., 2013. Mesozoic Tectonic Regimes and Regional Ore-Forming Background in NE China: Constraints from Spatial and Temporal Variations of Mesozoic Volcanic Rock Associations. *Acta Petrologica Sinica*, 29: 339–353. https://doi.org/10.1016/j.sedgeo.2012.12.001 (in Chinese with English Abstract)

Xu, Y., Chen, H. L., Zhang, F. Q., et al., 2010. The Upper Age Limitation of Mesozoic Lithospheric Thinning in NE China: Chronology Restriction of Yingcheng Formation in Songliao Basin. *Chinese Journal of Geology*, 1: 194–206 (in Chinese with English Abstract)

Yan, G. H., Mu, B. L., Xu, B. L., et al., 2000. The Chronology, Sr, Nd and Pb Isotopic Characteristics and Significance of the Triassic Alkaline Iintrusive Rocks of Yanliao-Yinshan Area. *Science in China Series D*: *Earth Sciences*, 30(4): 383–387. https://doi.org/10.1360/zd2000-30-4-383 (in Chinese)

Yang, J. H., Wu, F. Y., Chung, S. L., et al., 2006. A Hybrid Origin for the Qianshan A-Type Granite, Northeast China: Geochemical and Sr-Nd-Hf Isotopic Evidence. *Lithos*, 89(1/2): 89–106. https://doi.org/10.1016/j.lithos.2005.10.002

Zhang, J. H., 2009. Geochronology and Geochemistry of the Mesozoic Volcanic Rocks in the Great Xing'an Range, Northeastern China: [Dissertation]. China University of Geosciences, Wuhan (in Chinese with English Abstract)

Zhang, J. H., Ge, W. C., Wu, F. Y., et al., 2008. Large-Scale Early Creta-

ceous Volcanic Events in the Northern Great Xing'an Range, Northeastern China. *Lithos*, 102(1/2): 138–157. https://doi.org/10.1016/j.lithos.2007.08.011

Zhang, L. Q., Shao, J. A., 1998. Metamophic Core Complex in Ganzhuermiao, Inner Mongolia. *China Journal of Geology*, 2: 140–146 (in Chinese with English Abstract)

Zhang, Q. F., Pang, Y. M., Yang, S. F., et al., 2007. Geochronology of Zircon SHRIMP, Geochemistry and Its Implcation of the Volcanic Rocks from Yingcheng Formation in Depression Area, North of Songliao Basin. *Acta Geologica Sinica*, 81: 1248–1258. https://doi.org/10.1016/s1872-5791(07)60044-x (in Chinese with English Abstract)

Zhang, X. B., Wang, K. Y., Wang, C. Y., et al., 2017. Age, Genesis, and Tectonic Setting of the Mo-W Mineralized Dongshanwan Granite Porphyry from the Xilamulun Metallogenic Belt, NE China. *Journal of Earth Science*, 28(3): 433–446. https://doi.org/10.1007/s12583-016-0934-1

Zhang, X. Z., Yang, B. J., Wu, F. Y., 2006. The Lithosphere Structure in the Hingmong-Jihei (Hinggan-Mongolia-Jilin-Heilongjiang) Region, Northeastern China. *Geology of China*, 33: 816–823. https://doi.org/10.3969/j.issn.1000-3657.2006.04.011 (in Chinese with English Abstract)

Zhang, Y. L., Ge, W. C., Liu, X. M., et al., 2008. Isotopic Characteristics and Its Significance of the Xinlin Town Pluton, Great Hinggan mountains. *Journal of Jilin University*: *Earth Science Edition*, 38: 177–186. https://doi.org/10.3969/j.issn.1671-5888.2008.02.001 (in Chinese with English Abstract)

Zhang, Y. T., Zhang, L. C., Yin, J. F., et al., 2007. Geochemstry and Source Characteristics of Early Cretaceous Volcanic Rocks in Tahe, North Da Hinggan Mountain. *Acta Petrologica Sinica*, 23: 2811–2822. https://doi.org/10.1016/j.sedgeo.2007.05.003 (in Chinese with English Abstract)

Zhao, L. M., Takasu, A., Liu, Y. J., et al., 2017. Blueschist from the Toudaoqiao Area, Inner Mongolia, NE China: Evidence for the Suture between the Ergun and the Xing'an Blocks. *Journal of Earth Science*, 28(2): 241–248. https://doi.org/10.1007/s12583-017-0721-0

Zhao, L., Gao, F. H., Zhang, Y. L., 2013. Zircon U-Pb Chronology and Its Geological Implications of Mesozoic Volcanic Rocks from the Hailaer Basin. *Acta Petrologica Sinica*, 29: 864–874. https://doi.org/10.2307/628988

Zhao, X. C., Zhou, W. X., Fu, D., et al., 2018. Isotope Chronology and Geochemistry of the Lower Carboniferous Granite in Xilinhot, Inner Mongolia, China. *Journal of Earth Science*, 29(2): 280–294. https://doi.org/10.1007/s12583-017-0942-2